THE ANATOMICAL RECORD 300:171–195 (2017)

The Biomechanics of Bony Facial "Buttresses" in South African Australopiths: An Experimental Study Using Finite Element Analysis

JUSTIN A. LEDOGAR,[1,2]* STEFANO BENAZZI,[3,4] AMANDA L. SMITH,[2,5] GERHARD W. WEBER,[6] KEELY B. CARLSON,[7] PAUL C. DECHOW,[8] IAN R. GROSSE,[9] CALLUM F. ROSS,[10] BRIAN G. RICHMOND,[4,11] BARTH W. WRIGHT,[12] QIAN WANG,[8] CRAIG BYRON,[13] KRISTIAN J. CARLSON,[14,15] DARRYL J. DE RUITER,[7,15] LESLIE C. PRYOR MCINTOSH,[8] AND DAVID S. STRAIT[2,5]

[1]Zoology Division, School of Environmental and Rural Science, University of New England, Armidale, NSW, 2351, Australia
[2]Department of Anthropology, University at Albany, Albany, New York
[3]Department of Cultural Heritage, University of Bologna, Ravenna 48121, Italy
[4]Department of Human Evolution, Max Planck Institute for Evolutionary Anthropology, Leipzig 04103, Germany
[5]Department of Anthropology, Washington University in St. Louis, St. Louis, Missouri
[6]Department of Anthropology, University of Vienna, Vienna A-1090, Austria
[7]Department of Anthropology, Texas A&M University, College Station, Texas
[8]School of Science and Mathematics, Abraham Baldwin Agricultural College, Tifton, Georgia 30605
[9]Department of Mechanical and Industrial Engineering, University of Massachusetts, Amherst, Massachusetts
[10]Department of Organismal Biology and Anatomy, University of Chicago, Chicago, Illinois
[11]Division of Anthropology, American Museum of Natural History, New York, New York
[12]Department of Anatomy, Kansas City University of Medicine and Biosciences, Kansas City, Missouri
[13]Department of Biology, Mercer University, Macon, Georgia
[14]Department of Cell and Neurobiology, Keck School of Medicine, University of Southern California, Los Angeles, California
[15]Evolutionary Studies Institute, University of the Witwatersrand, Wits 2050, South Africa

ABSTRACT

Australopiths exhibit a number of derived facial features that are thought to strengthen the face against high and/or repetitive loads associated with a diet that included mechanically challenging foods. Here, we use finite element analysis (FEA) to test hypotheses related to the purported strengthening role of the zygomatic root and "anterior pillar" in australopiths. We modified our previously constructed models of Sts 5 (*Australopithecus africanus*) and MH1 (*A. sediba*) to differ in the morphology of the zygomatic root, including changes to both the shape and positioning of the zygomatic root complex, in addition to creating variants of Sts 5 lacking anterior pillars. We found that both an expanded

Grant sponsor: National Science Foundation Physical Anthropology HOMINID Program; Grant numbers: NSF BCS 0725219, 0725183, 0725147, 0725141, 0725136, 0725126, 0725122, 0725078; Grant sponsor: National Science Foundation "Biomesh"; Grant number: NSF DBI 0743460; Grant sponsors: EU FP6 Marie Curie Actions; SUNY Albany Dissertation Research Fellowship; SUNY Albany GSEU Professional Development Grant.

*Correspondence to: Justin A. Ledogar, Zoology Division, School of Environmental & Rural Science, University of New England, Armidale, NSW, Australia. E-mail: jledogar@gmail.com

Received 12 March 2016; Revised 29 August 2016; Accepted 6 September 2016.

DOI 10.1002/ar.23492

Published online in Wiley Online Library (wileyonlinelibrary.com).

zygomatic root and the presence of "anterior pillars" reinforce the face against feeding loads. We also found that strain orientations are most compatible with the hypothesis that the pillar evolved to resist loads associated with premolar loading, and that this morphology has an ancillary effect of strengthening the face during all loading regimes. These results provide support for the functional hypotheses. However, we found that an anteriorly positioned zygomatic root increases strain magnitudes even in models with an inflated/reinforced root complex. These results suggest that an anteriorly placed zygomatic root complex evolved to enhance the efficiency of bite force production while facial reinforcement features, such as the anterior pillar and the expanded zygomatic root, may have been selected for in part to compensate for the weakening effect of this facial configuration. Anat Rec, 300:171–195, 2017. © 2016 Wiley Periodicals, Inc.

Key words: zygoma; function; evolution

The australopiths are extinct early humans (hominins) known from the Plio-Pleistocene of Africa. Most australopith species (i.e., those within the genera *Australopithecus* and *Paranthropus*) are characterized by highly derived craniodental traits, including massive cheek teeth with thick enamel and masticatory muscles that evidently were large and/or positioned so as to have a high leverage for generating bite force (e.g., Rak, 1983; Demes and Creel, 1988; Smith et al., 2015a). Additionally, australopiths exhibit a number of derived facial features that are thought to strengthen the face against high and/or repetitive loads associated with a diet that included mechanically challenging foods (i.e., those whose mechanical properties make them difficult to eat; Rak, 1983; Strait et al., 2009; Smith et al., 2015a). These purported facial reinforcement features, which vary in their expression both within and among australopith species, are hypothesized to confer structural strength to the facial skeleton during biting and chewing. A lively debate has ensued concerning whether or not these bony facial features are adaptations for feeding on either hard or compliant/tough foods, but there is widespread agreement that they collectively represent feeding and/or dietary adaptations of some kind (Teaford and Ungar, 2000; Strait et al., 2009, 2012, 2013; Grine et al., 2010; Ungar et al., 2010; Cerling et al., 2011; Scott et al., 2012). However, the degree to which purported facial "buttresses" confer structural strength to the facial skeleton during feeding has not been fully evaluated because the geometrical complexity of the face makes these hypotheses difficult to test. This article examines the biomechanical/functional role of two such facial "buttresses" in australopiths: the inflated/expanded zygomatic root and the "anterior pillar."

Note that, as discussed by Prado et al. (this issue), true buttresses are defined as horizontal structures that resist forces transmitted via vertically oriented pillars. For example, Sicher and Tandler (1928) hypothesized that, during biting, forces are transmitted from the bite point superiorly along canine-frontal and zygomatic pillars, both of which are supported by supra- and infraorbital buttresses. However, Prado et al. (this issue) demonstrate that craniofacial deformation regimes in humans and other primates are much more complex than simple models of pillars and buttresses. Therefore, we prefer to use "reinforce" or "strengthen" as opposed to "buttress" when discussing the purported function of the zygomatic root and anterior pillars.

Rak (1983) suggested that the size and shape of the zygomatic root and its placement relative to the rostrum played a key role in influencing strain patterns in the australopith facial skeleton. With respect to its shape, he argued that a deep and/or laterally expanded zygomatic root complex (ZRC) with a straight and steeply inclined zygomaticoalveolar crest (ZAC) may act to reinforce the face against feeding loads. Among australopith species, members of the genus *Paranthropus* exhibit the most expanded/straight zygomatic roots. The ZAC is curved in *A. afarensis* (Kimbel et al., 2004), but ZAC shape is more variable in *A. africanus*, with Sts 5 having a somewhat curved morphology and most other individuals (e.g., Sts 52 and Sts 71) having those that are more straight/steep. A straight and steeply inclined ZAC is also present in the holotype cranium (MH1) of *A. sediba* (Berger et al., 2010). In living primates, most species exhibit a curved ZAC, including most chimpanzees and gorillas (Kimbel et al., 2004). However comprehensive comparative studies of ZAC shape and its role in feeding biomechanics have yet to be conducted (but see Weber and Krenn, this issue).

The placement of the ZRC in relation to the tooth rows is also hypothesized to have played a role in masticatory stress resistance in australopiths. In addition to increasing the mechanical advantage (i.e., leverage) of the jaw adductor muscles, Rak (1983) suggested that an anteriorly placed zygomatic root could further strengthen the face against the forces generated at the bite point, especially during feeding behaviors involving the premolars and anterior teeth (see also Hylander, 1977). Among australopiths, the most anteriorly positioned ZRCs are present in *Paranthropus*. Most *A. africanus* individuals also exhibit a somewhat anteriorly positioned ZRC, as well as *A. sediba* (Berger et al., 2010; Weber and Krenn, this issue), whereas posterior positioning is found in *A. afarensis* (Kimbel et al., 2004). However, like ZAC shape, ZRC position varies within *A.*

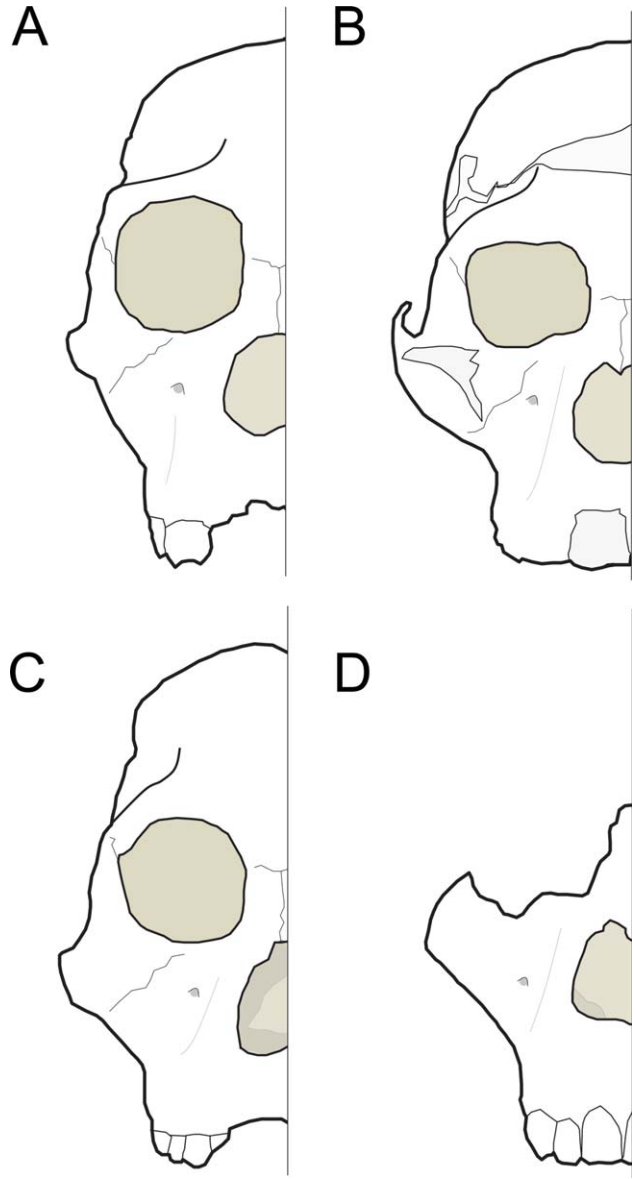

Fig. 1. *Australopithecus sediba* (MH1, **A**) and *A. africanus* (Sts 5, **B**; Sts 71, **C**; Sts 52, **D**) showing variation in the shape of the zygomatic root (ZR)/zygomaticoalveolar crest (ZAC) between and within australopith species. Sts 5 exhibits a curved ZAC, whereas other *A. africanus* individuals and *A. sediba* exhibit a straight/steep ZAC.

africanus with some individuals (e.g., Sts 52 and Sts 71) exhibiting an anterior migration, while others (e.g., Sts 5) have a greater proportion of the snout protruding beyond the root. Although comparative studies examining the effects of root positioning (or shape) on craniofacial strength have yet to be conducted in living primates, species that include mechanically challenging foods in their diet have been shown to exhibit more anteriorly positioned ZRCs in order to increase their mechanical advantage during biting (e.g., capuchins and sakis; Wright, 2005).

The so-called anterior pillars (AP, sometimes called "nasal pillars"), expressed to varying degrees in *A. africanus* and *Paranthropus robustus* (and possibly *P. boisei*; see Rak, 1983, 1985a,1985b,1985c; Villmoare and Kimbel, 2011), are prominent bony "columns" that run vertically along the nasal aperture that are also purported to have played a role in resisting feeding loads. Particularly in reference to *A. africanus*, citing its "molarized" premolars, Rak (1983, 1985a,b,c) likened the anterior pillars to struts that resist compressive stresses during premolar-focused biting. Such foods could have included unripe fruits, hard nuts, and/or seeds that require premolar processing before mastication of the softer inner tissues by the molar teeth (Peters, 1987; Strait et al., 2009). These food items are also consistent with the bunodont postcanine teeth exhibited by *A. africanus* and other australopith species, which are poorly suited for a diet of tough, displacement limited (Lucas et al., 2000) foods (Teaford and Ungar, 2000; Strait et al., 2013). However, the pillars also have been suggested to potentially represent an adaptation for nondietary behaviors including oral prehension using the canines and incisors (McKee, 1989). Recently, Villmoare and Kimbel (2011) examined the internal morphology of the anterior pillar and defined the feature more expansively to represent essentially the junction where the outer wall of the maxilla "turns" into the aperture to meet the lateral wall of the nasal cavity. Using such a definition, all primates have an anterior pillar along the margins of the nasal aperture. This study, however, adopts a more restrictive definition in which the pillar is a distinctive topographic feature of the maxilla manifesting itself as a blunt "ridge" seen externally.

Strait et al. (2009) examined the feeding biomechanics of *A. africanus* using FEA. They found that the pillar was subjected to large compressive forces during premolar, but not molar, biting. They also found that compressive strains were primarily oriented along the long axis of the pillar. Further, a model of *Macaca fascicularis* was found to deform under premolar loading in a much different fashion, with a combination of variably oriented tensile and compressive strains surrounding the alveolus of the loaded premolar and near the nasal margin. From these results, Strait et al. (2009) concluded that the facial configuration of *A. africanus* is consistent with the biomechanical and dietary hypotheses put forward by Rak (1983). More recently, Smith et al. (2015a,b) found that premolar loading produced elevated compressive strains directed parallel to the nasal margin in *A. africanus, Paranthropus boisei*, and a sample of six *Pan troglodytes*. This, too, is consistent with Rak's (1983) model, which implicitly assumes that the nature of the deformation experienced by the rostrum during premolar bites is the same in hominins (and, presumably, nonhominin apes) with and without pillars.

Interestingly, strain magnitudes in the pillar are higher in *A. africanus* than in the other taxa (Smith et al., 2015a), which seems counter-intuitive if the pillar is a stress-reducing trait. One interpretation of this finding could be that the hypothesis that the pillar has evolved as a stress-reducing trait must be wrong. For example, Grine et al. (2010) take the position that high strains indicate that the pillar cannot be an adaptation to withstand premolar loads, because if it was then strains would certainly be low. Indeed, strains are low in the pillar during molar loading, so they suggest that molar loading is a better explanation for the evolution of the pillar than premolar loading. This hypothesis

TABLE 1. List of anatomical landmarks and curves of the template for TPS warping

Paired landmarks	Unpaired landmarks	Curve name	#	Smlndmk count[a]
Anterior eminence (ae)	Glabella (g)	Frontotemporal-zygomatic left	1	15
Jugale (ju)	Incisive foramen (if)	Frontotemporal-zygomatic right	2	15
Lacrimal (la)[b]	Int-alv-proc (iap)	Internal alveolar process left	3	7
I1[c]	Prosthion (pr)	Internal alveolar process right	4	7
I2[c]	Rhinion (rh)	Lower zygomatic arch left	5	20
C[c]	Staphylion (sta)	Lower zygomatic arch right	6	20
P3[c]		Nasal aperture left	7	8
P4[c]		Nasal aperture right	8	8
M1[c]		Orbital rim left	9	19
M2[c]		Orbital rim right	10	19
M2-int[d]		Upper zygomatic arch left	11	10
		Upper zygomatic arch right	12	10
		Total semilandmarks on curves:		**158**

[a]Semilandmarks identified on the curves.
[b]Approximately at the level of the anterior lacrimal crest.
[c]External alveolar process at the level of the mid-buccal cervix.
[d]Internal alveolar process at the level of the mid-buccal cervix.

predicts that the anterior pillar is more effective at resisting molar loading than premolar loading. Alternatively, one might infer that strain along the nasal aperture is high during premolar loading and thus natural selection is likely to act on the size and shape of that region because such regions are structurally more at risk (Strait et al., 2009, 2013; Ross et al., 2011; Ross and Iriarte-Diaz, 2014; Smith et al., 2015a). This interpretation implies that strains are high in the pillar but would be even higher in the region if the pillar were absent (all other things being equal).

We test hypotheses related to the purported strengthening role of the zygomatic root complex (ZRC) and anterior pillar (AP) in *A. africanus* and *A. sediba* using finite element analysis (FEA) by modifying our previously constructed finite element models (FEMs) of Sts 5 (Strait et al., 2009; Smith et al., 2015a) and MH1 (Ledogar et al., 2016a), respectively. These specimens differ in the bony morphology of the zygomatic and nasal margin. Specifically, the zygomaticoalveolar crest (ZAC) is straight and steeply inclined in MH1 but somewhat more curved in Sts 5 (although not as curved as in many other hominins, such as *Homo habilis*). However, as discussed above, this feature is variable in *A. africanus*, with specimens such as Sts 52 and Sts 71 having zygomatics more similar in shape to MH1 (Fig. 1). In addition to shape, there are differences in the relative positioning of the ZRC between MH1 and Sts 5, with the ZRC being situated above the mesial border of the first molar in MH1 (Berger et al., 2010) but positioned above the second molar in Sts 5. However, as discussed above, ZRC position varies within *A. africanus*, with Sts 5 exhibiting a more posteriorly positioned ZRC compared to other individuals, including Sts 52 and Sts 71. With respect to the AP, Sts 5 exhibits the most pronounced pillars of all *A. africanus* individuals (Lockwood, 1999), whereas pillars are lacking in MH1. However, like zygomatic morphology, the presence or absence of the anterior pillars among *A. africanus* individuals is variable (Rak, 1983, 1985a,b,c; McKee, 1989; Lockwood, 1999), with some specimens possessing reduced pillars (e.g., TM-1512) and some with large and prominent pillars (e.g., Sts 5).

A particular strength of FEA is the ability to examine the functional consequences of changes in individual features by comparing variants of a single model that differ in select aspects of shape but are otherwise identical (e.g., Strait et al., 2007; Stayton, 2009; Panagiotopoulou et al., 2011; Benazzi et al., 2013, 2015; Dumont et al., 2014). We examined the effects of modifying the ZRC of Sts 5 to be similar in morphology (shape and placement) to MH1, and vice versa. We test the hypothesis (Hypothesis 1) that a more inflated and/or anteriorly-placed ZRC confers structural strength to the face in both species. We also examine the consequences of "removing" the anterior pillar in Sts 5 to test the hypothesis (Hypothesis 2) that the presence of "anterior pillars" in *A. africanus* strengthens the face against occlusal loads. Hypothesis 2 further predicts that the strengthening effect of the anterior pillar is most evident in reducing loads during premolar (versus molar) biting. An alternative (Hypothesis 3) predicts the opposite, namely, that the pillar has a greater effect in reducing molar rather than premolar loads.

MATERIALS AND METHODS

Model Construction: Zygomatic Variants

To test the predictions of Hypothesis 1, we examined four variants each of our previously constructed models of *A. africanus* (Sts 5) and *A. sediba* (MH1), for a total of eight models. These included the unmodified originals (UNMOD) and three variants per species that were modified to differ in the shape (S-MOD), position (P-MOD), or both shape and position (SP-MOD) of the ZRC. These resulted in variants that had either: a curved ZAC and posteriorly positioned ZRC, a curved ZAC and anteriorly positioned ZRC, a straight/steep ZAC and posteriorly positioned ZRC, or a straight/steep ZAC and anteriorly placed ZRC. These combinations represent those found in known species, as well as some hypothetical combinations, both of which are useful in the evaluation of Rak's (1983) functional hypothesis (see Discussion below).

For Sts 5 model variants, one was modified to have a straight/steep ZAC similar to that of MH1 UNMOD (Sts 5 S-MOD), a second was modified to have the ZRC positioned above M^1 as in MH1 UNMOD (Sts 5 P-MOD), and a third was modified to have both a straight/steep ZAC and more anteriorly placed ZRC (Sts 5 SP-MOD). According to Hypothesis 1, these modifications are all

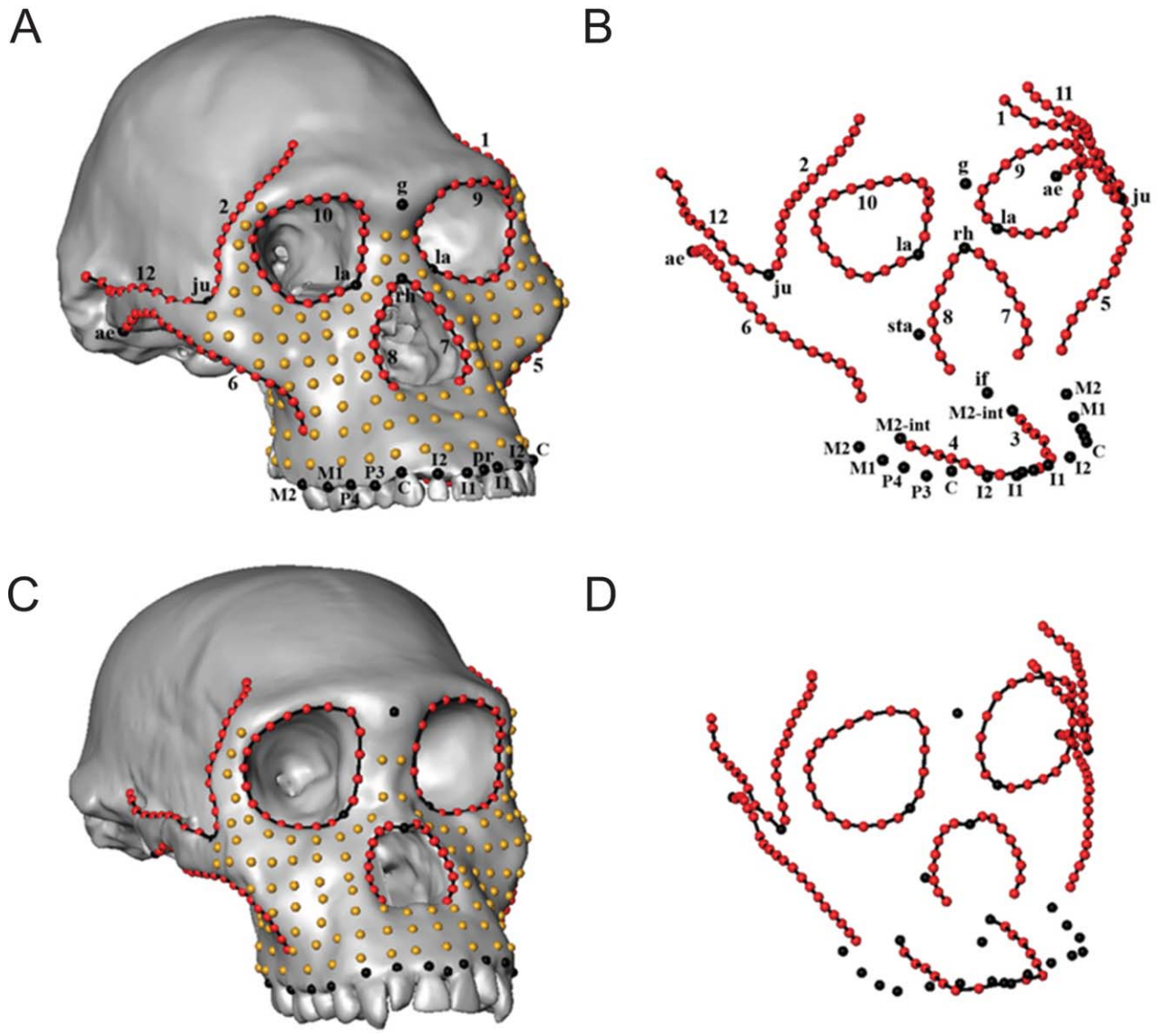

Fig. 2. Landmarks and templates used in TPS warping of Sts 5 (**A**, **B**) and MH1 (**C**, **D**). Labels refer to Table 1.

predicted to strengthen the face, meaning that strains should be lower in the modified crania than in the unmodified model. Inversely, for the MH1 model variants, one was modified to have a curved ZAC similar to that of Sts 5 UNMOD (MH1 5 S-MOD), a second was modified to have the ZRC positioned above M^2 as in Sts 5 UNMOD (MH1 P-MOD), and a third was modified to have both a curved ZAC and posteriorly placed ZRC (MH1 SP-MOD). Hypothesis 1 predicts that these modifications will weaken the face, meaning that strains should be higher in the modified crania than in the unmodified model.

To generate the S-MOD and P-MOD variants in both species, 3D-templates of 28 landmarks and 283 semilandmarks were first created to capture the geometry of the complete facial surfaces of MH1 UNMOD and Sts 5 UNMOD using Viewbox (dHAL Software, Kifissia, Greece). The semilandmarks included 158 that followed 12 curves running along the margins of anatomical structures in addition to 125 that were selected on the facial surface of both crania (Table 1; Fig. 2). The template built on Sts 5 UNMOD was warped onto the MH1 UNMOD cranium by iterative thin-plate spline (TPS) algorithms (Bookstein, 1991), thus obtaining a corresponding (semi)landmark configuration onto MH1 UNMOD. This procedure aligns Sts 5 and MH1 according to homologous anatomical landmarks on both models, while semilandmarks were allowed to slide along curves and surfaces to minimize the bending energy of the TPS computed between them. Once relaxed (i.e., when the bending energy has been minimized), semilandmarks can be considered geometrically homologous points (Gunz, 2005).

To create surface models of MH1 S-MOD and Sts 5 S-MOD, the unmodified Sts 5 and MH1 models were considered alternatively the reference and the target

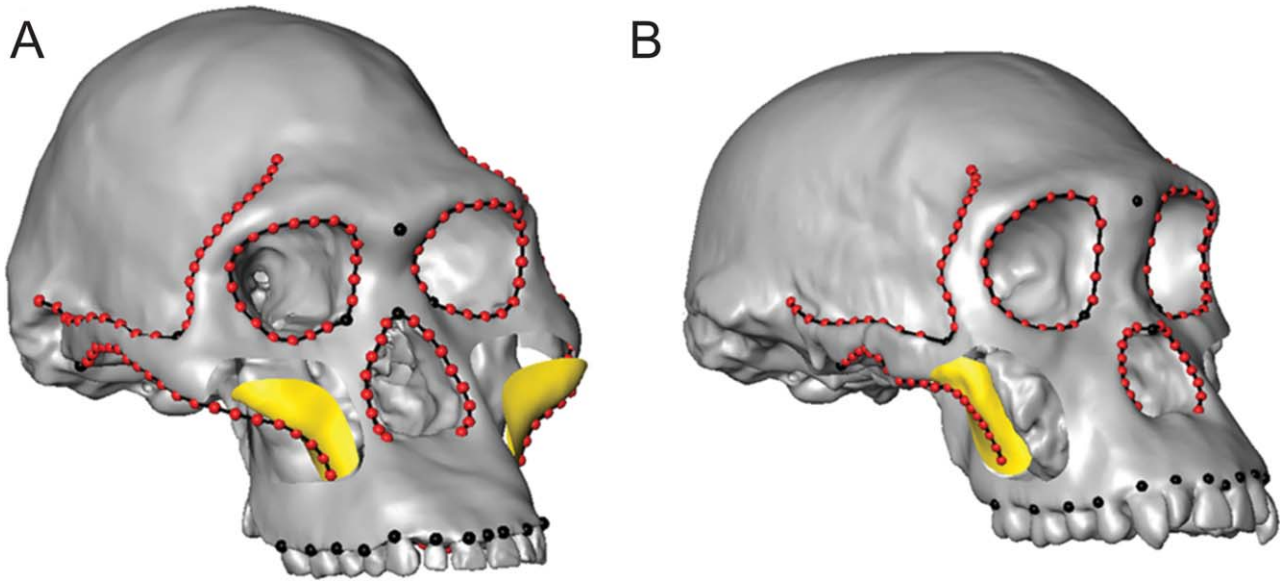

Fig. 3. (**A**) Anterior displacement of the zygomatic root (ZR) in Sts 5 to the level of M^1/P^4 (as in MH1), and (**B**) posterior displacement of the ZR in MH1 to M^2 (as in Sts 5).

template, respectively. To obtain an Sts 5 (semi)landmark configuration with MH1 zygomatic root shape (i.e., straight/steep ZAC), as well as a MH1 configuration with Sts 5 zygomatic root shape (i.e., curved ZAC), the reference template (MH1 and Sts 5, respectively) was warped onto the target template (Sts 5 and MH1, respectively), declaring the semilandmarks that fell onto the zygomatic root as missing. Their position was estimated according to the minimum bending energy requirement of the TPS during the sliding step. In Avizo 7 software (Visualization Sciences Group), the 311 (semi)landmarks of the reference template (MH1 and Sts 5, respectively) were thus transformed into the corresponding (semi)landmarks of the target using the TPS functions, whereas the surface of the reference was interpolated so as to minimize the bending energy of the relative transformation. Finally, the zygomatic roots of MH1 and Sts 5 were removed in Rapidform XOR2 (INUS Technology, Seoul, Korea) and substituted with the zygomatic roots obtained from the resulting warped surface (MH1 S-MOD and Sts 5 S-MOD, respectively).

To create surfaces of MH1 P-MOD and Sts 5 P-MOD, the morphology of the zygomatic root was preserved, but the position of the root was changed. For MH1 P-MOD, the zygomatic root of unmodified MH1 (originally placed at the level of M^1/P^4) was digitally isolated and displaced backward to the level of the LM^2 (as in Sts 5). For Sts 5 P-MOD, the zygomatic root of the unmodified Sts 5 (originally placed at the level of the LM^2) was digitally isolated and displaced forward to the level of M^1/P^4 (as in MH1). The template of (semi)landmarks built on MH1 was then warped onto the modified (zygomatic root displaced backward) MH1 digital model, while the template built on Sts 5 was warped onto the modified (zygomatic root displaced forward) Sts 5 digital model using the TPS functions (Fig. 3). The position of the semilandmarks that fell near the "new" zygomatic root was estimated, but the shape of the other facial features (such as the nasal aperture, the inferior orbital rim, the alveolar process of the maxilla, the frontotemporal line, the upper zygomatic arch) was constrained. In Avizo, the (semi)landmarks of the reference templates were then transformed into the corresponding (semi)landmarks of the targets, whereas the surface of the reference was interpolated so as to minimize the bending energy of the relative transformation. Two new digital models (MH1 P-MOD and Sts 5 P-MOD) were then obtained.

To create surfaces of MH1 SP-MOD and Sts 5 SP-MOD, both the shape and the position of the zygomatic root were modified. To obtain the new models, the zygomatic roots of MH1 P-MOD and Sts 5 P-MOD were removed in Rapidform XOR and substituted with the zygomatic roots of MH1 S-MOD and Sts 5 S-MOD, respectively.

With respect to the internal architecture of the modified models, we have modeled trabecular bone as watertight volumes of bone, one zygo-frontal volume and one maxillary volume, as opposed to individual trabeculae, consistent with our previous analyses (see Smith et al., 2015a,b; Ledogar et al., 2016a,b). In our modified models of both Sts 5 and MH1, trabecular volumes were also modified in order to maintain similar cortical bone thickness across the model variants. We did not warp the internal structure of Sts 5 to that of MH1, or vice versa, thus focusing our comparisons on the external geometry of the ZRC. Likewise, we did not examine the effects of altering the shape of the trabecular volumes in either specimen. Variation in the internal architecture of the face may play an important role in feeding biomechanics (e.g., Villmoare and Kimbel, 2011). For example, one might predict an increase in strength (and thus a decrease in strain magnitudes) when the cortical bone of the ZRC is thickened internally, leaving the external morphology of the ZRC unaltered. However, we do not test this hypothesis here as the morphologies in question obviously manifest themselves externally.

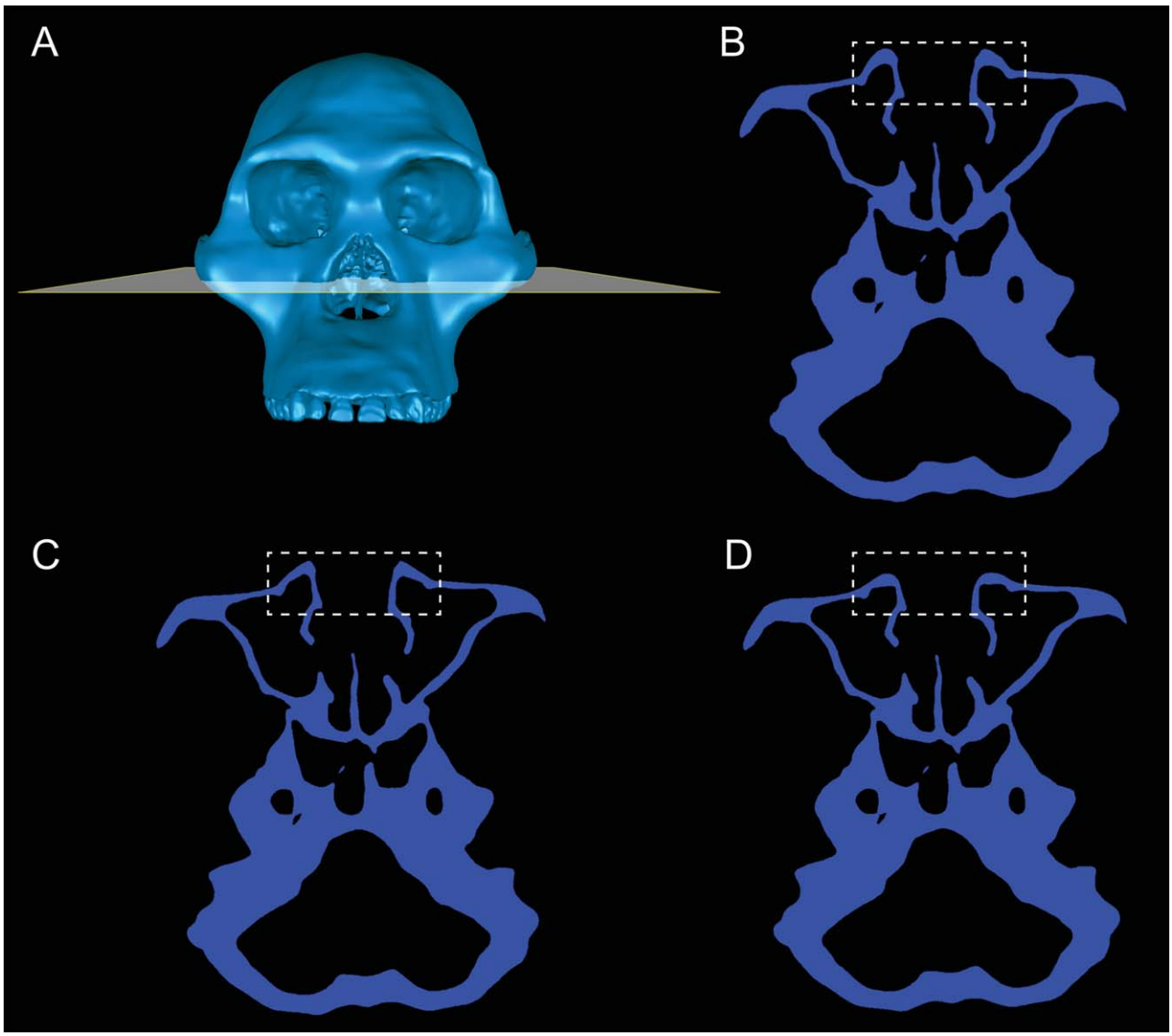

Fig. 4. Cutting plane (**A**) and cross-section through the anterior pillars of the unmodified model of Sts 5 (**B**), Sts 5 NP-1 (**C**), and Sts 5 NP-2 (**D**), highlighting the pillar modifications.

Model Construction: Pillar Variants

To test the predictions of Hypotheses 2 and 3, we examined two variants of our previously constructed model of *A. africanus* (Sts 5 UNMOD), both with the anterior pillars digitally "removed" in slightly different ways. Villmoare and Kimbel (2011) analyzed the pillar of *A. africanus* using CT data and found that its structure is similar to a hollow tube as opposed to being solid. Similarly, in our model of Sts 5 UNMOD, the pillars are represented by hollow "columns" of bone that surround a pocket of the anterior aspect of the maxillary sinus cavity, although the maxillary sinus does not strongly invaginate the pillar towards its inferior most extent, near the inferior margin of the nasal aperture. Thus, they are modeled here, as well as by Strait et al. (2009), as curved plates of bone. Note that Villmoare and Kimbel (2011) incorrectly characterized the pillar in our model of Sts 5 (Strait et al., 2009) as being solid (Villmoare, pers. comm.)

To create "No-Pillar" variants of Sts 5, the nasal margin of the original Sts 5 UNMOD surface model was manually edited using a combination of cutting, sanding, and smoothing procedures in Geomagic Studio 2012 (Research Triangle Park, NC). These variants are heuristic, but the modifications were geometrically so simple that they nonetheless serve a useful purpose in investigating the mechanical consequences of pillar morphology. Both models had the pillars "removed" in slightly different ways. These models will hereafter be referred to as Sts 5 NP-1 and Sts 5 NP-2. For Sts 5 NP-1, the lateral bulge of the bony anterior pillar and corresponding maxillary sinus surface were flattened while preserving

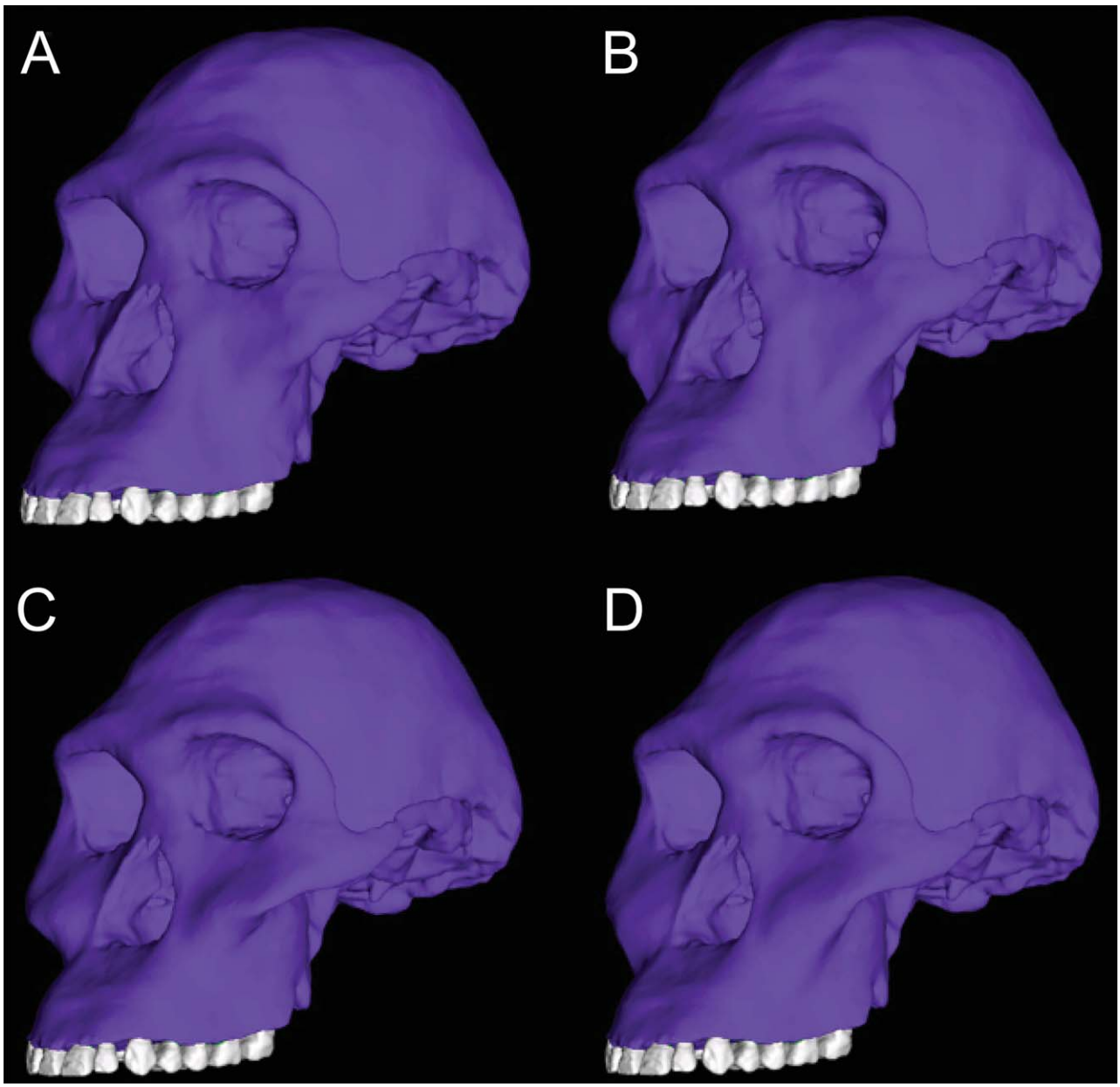

Fig. 5. (**A**) Original (unmodified) FEM of Sts 5, alongside warped variants (**B**) Sts 5 S-MOD, (**C**) Sts 5 P-MOD, and (**D**) Sts 5 SP-MOD.

the facial profile in lateral view. In this model, the cortical bone along the edge of the nasal margin still maintains a thickened ridge along the edge of the nasal margin. For Sts 5 NP-2, the pillars were "eroded" such that the outpocketing of the sinus is greatly reduced and the cortical bone of the anterior wall of the maxillary sinus, along the nasal margin, and entering the nasal cavity maintained a similar thickness. This model therefore did not preserve the lateral facial profile of the unmodified version. This erosion gave the model a nasal region that was concave in lateral view. Figure 4 shows the original and "No-Pillar" model variants of Sts 5 in cross section, highlighting modifications to the pillar. In both models, the thickness of cortical bone was maintained after removal of the pillar. Although we cannot be certain what Sts 5 would have looked like if, in life, it lacked pillars, it is likely that the two modified models examined here bracket a large proportion of the possible morphologies.

Creation of Solid Finite Element Models

Stereolithography (STL)-formatted surface meshes of all Sts 5 and MH1 variants were imported into the 3Matic module of Mimics v 14.0 (Materialise, Ann Arbor, MI) for solid (i.e., finite element) meshing. All models were meshed at similar densities using 4-noded tetrahedral elements. The solid models of Sts 5 zygomatic variants

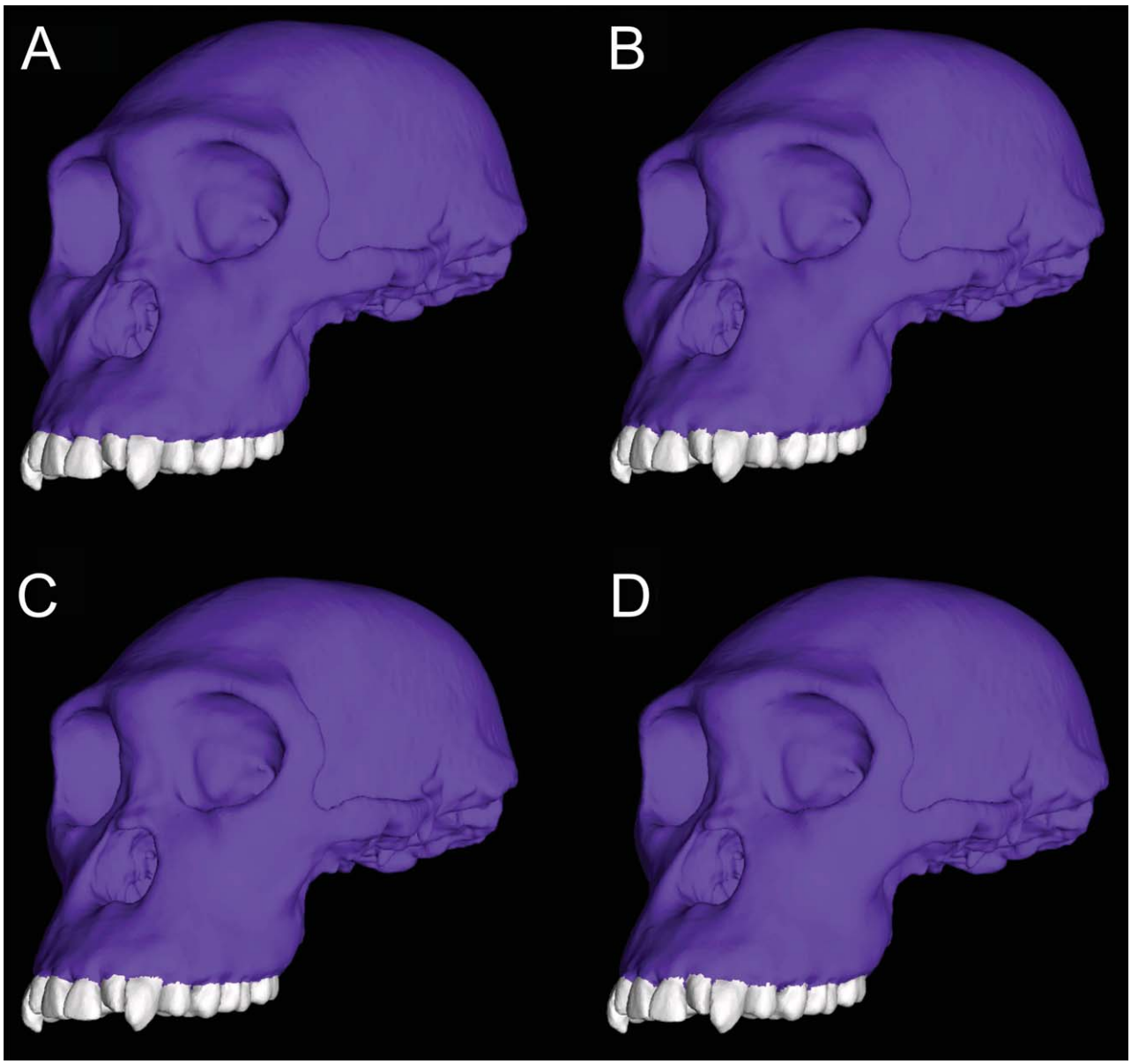

Fig. 6. (**A**) Original (unmodified) FEM of MH1, alongside warped variants (**B**) MH1 S-MOD, (**C**) MH1 P-MOD, and (**D**) MH1 SP-MOD.

(Fig. 5), MH1 zygomatic variants (Fig. 6), and Sts 5 pillar variants (Fig. 7) were then imported as Nastran (NAS) files into Strand7 (Strand7 Pty Ltd, Sydney, NSW) finite element software for assignment of material properties, constraints, and muscle loads. Full details on these procedures can be found elsewhere (Smith et al., 2015a,b). Briefly, a thermal diffusion method (Davis et al., 2011) was used to distribute isotropic but regionally variable material properties of modern ape craniofacial cortical bone from Smith et al. (2015b), while trabecular bone and enamel volumes were assigned properties as homogeneous and isotropic following the same study. All models were constrained at the two TMJs and a bite point for each biting simulation, which included a left first premolar (LP^3) and left second molar (LM^2) bite. Chewing muscle forces were applied to the models at maximal force (simulating a forceful, static bite) on both sides of the head using Boneload (Grosse et al., 2007), with individual muscle force vectors oriented toward insertion sites on the mandible. The variants of Sts 5 were loaded with chimpanzee muscle forces that were scaled to the volume$^{2/3}$ of Sts 5 UNMOD following the scaling procedures in Smith et al. (2015a,b). Similarly, model variants of MH1 were loaded with chimpanzee forces that were scaled to the volume$^{2/3}$ of MH1 UNMOD. As shown by Dumont et al. (2009), this scaling law removes size effects for a comparative analysis of stress and strain, since volume$^{2/3}$ is proportional to surface area.

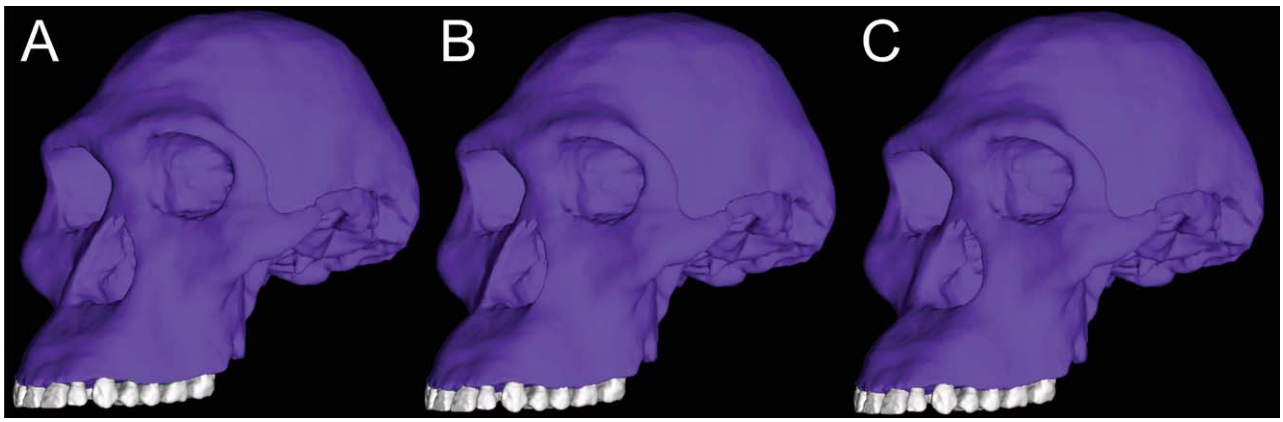

Fig. 7. The original (unmodified) FEM of Sts 5 (**A**) alongside two "No-Pillar" models of Sts 5 that have had the anterior pillars digitally removed in slightly different ways (see main text), Sts 5 NP-1 (**B**) and Sts 5 NP-2 (C).

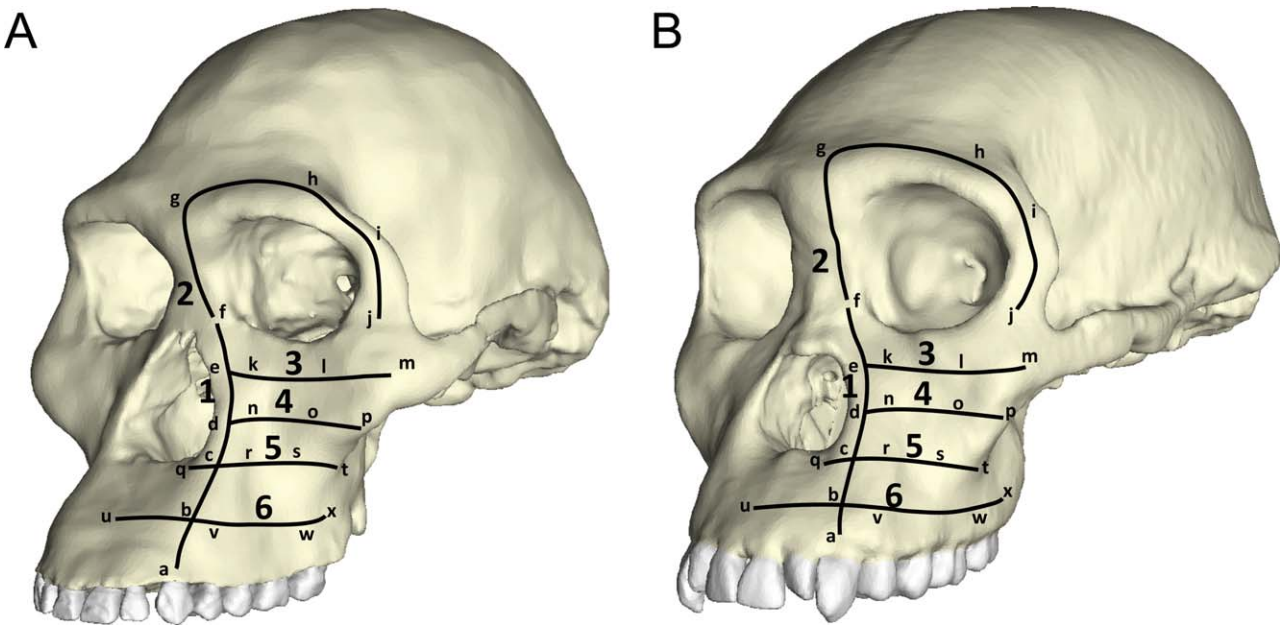

Fig. 8. FEMs of (**A**) Sts 5 UNMOD and (**B**) MH1 UNMOD showing the six line transects along which von Mises strain magnitudes were collected. Labels a–x represent various points along the transects.

Analysis of Model Output Parameters

The magnitude and spatial patterning of von Mises strain magnitudes generated during each biting simulation were compared across the model variants of Sts 5 and for MH1. To capture differences in strain magnitude and patterning between the two sets of FEMs, data on von Mises strain magnitudes were collected from points lying along six homologous line transects on the working (left) side of each model (Fig. 8). As opposed to comparing strains at individual points across the models, these transects provide a more nuanced view of the biomechanical consequences associated with each bony modification. In addition to strain magnitudes, data on bite force production, biting efficiency (i.e., leverage or mechanical advantage), and temporomandibular (TMJ) reaction forces were recorded and compared.

RESULTS

The Zygomatic Root Complex and Zygomaticoalveolar Crest

Color mapping of von Mises strain magnitudes in the model variants of Sts 5 (Fig. 9) and MH1 (Fig. 10) illustrates the effects of modifying the shape, modifying the

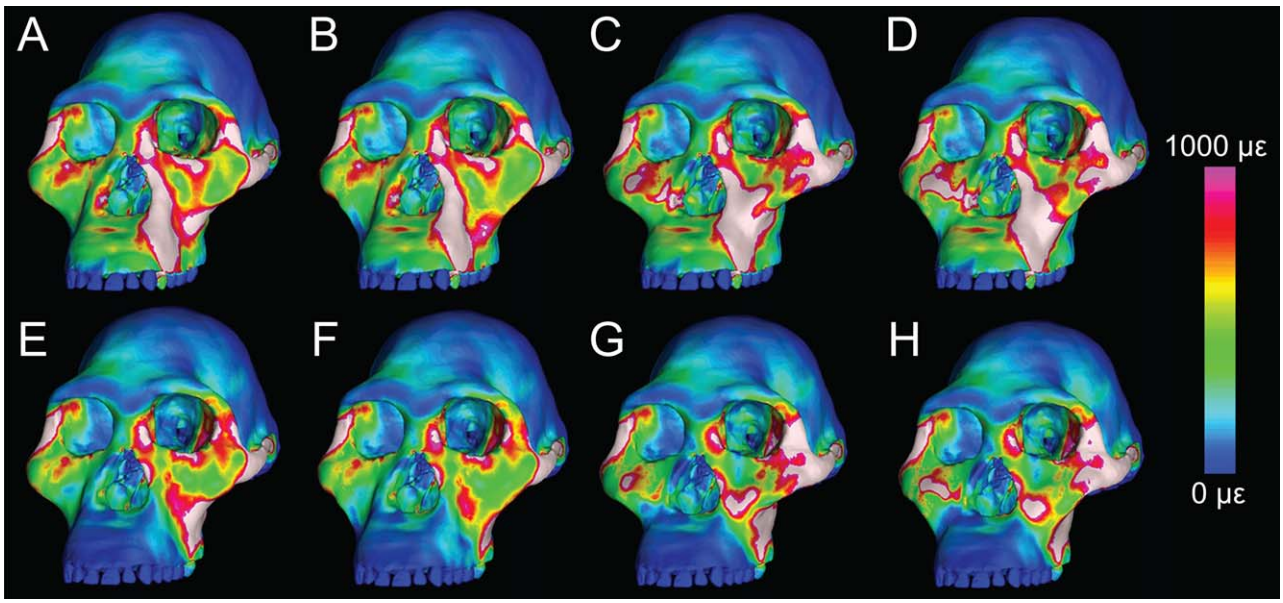

Fig. 9. FEMs of Sts 5 UNMOD (**A**, **E**), Sts 5 S-MOD (**B**, **F**), Sts 5 P-MOD (**C**, **G**), and Sts 5 SP-MOD (**D**, **H**) showing the magnitude of von Mises strains during simulations of LP^3 (top row) and LM^2 (bottom row) biting. The von Mises strain is shown at a scale of 0 to 1000 με. White regions exceed scale.

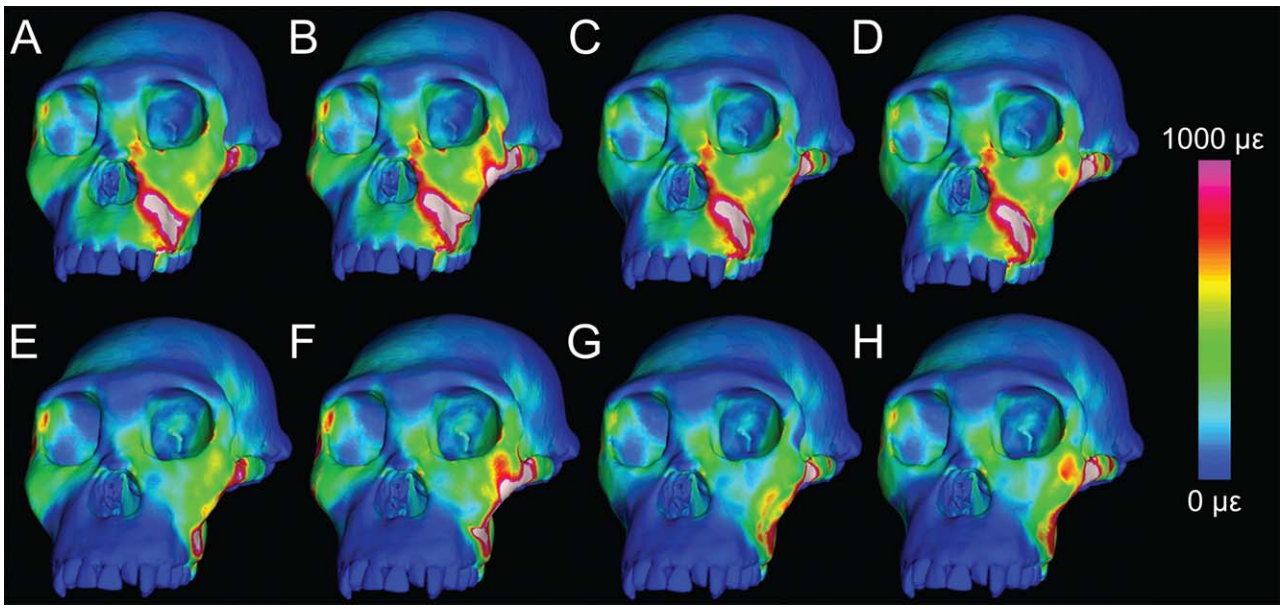

Fig. 10. FEMs of MH1 UNMOD (**A**, **E**), MH1 S-MOD (**B**, **F**), MH1 P-MOD (**C**, **G**), and MH1 SP-MOD (**D**, **H**) showing the magnitude of von Mises strains during simulations of LP^3 (top row) and LM^2 (bottom row) biting. The von Mises strain is shown at a scale of 0 to 1000 με. White regions exceed scale.

position, and modifying both the shape and position of the zygomatic root. Some facial regions of these FEMs exhibited large differences in strain magnitude between the models, including the nasal margin, postorbital bar, zygomatic body, and zygomatic root, while other regions experienced little or no difference, such as the supraorbital tori. In general, results show that the presence of a straight and steeply inclined zygomaticoalveolar crest (ZAC) reduces strain magnitudes across many facial regions, consistent with predictions. In particular, strain magnitudes in Sts 5 decrease when the ZAC is straightened (Fig. 9b,f), but increase in MH1 when the ZAC is curved (Fig. 10b,f). However, in contrast to predictions, models with an anteriorly-positioned zygomatic root complex experienced larger strain magnitudes in many areas of the face relative to the unmodified Sts 5,

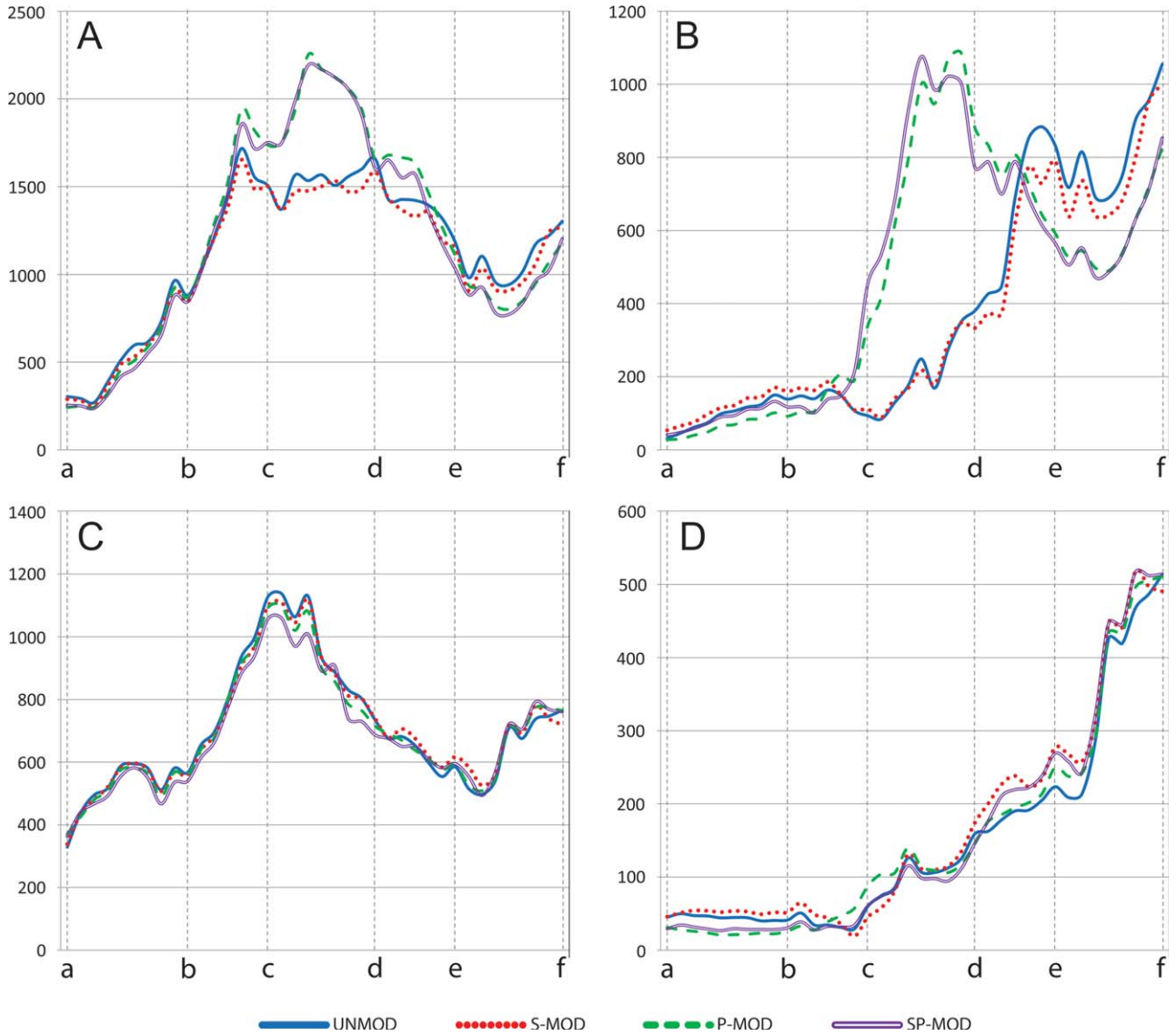

Fig. 11. Line graphs showing differences in the von Mises microstrain (*y*-axis) along Transect 1 between UNMOD, S-MOD, P-MOD, and SP-MOD variants of Sts 5 during (**A**) LP^3 and (**B**) LM^2 biting, and model variants of MH1 during (**C**) LP^3 and (**D**) LM^2 biting. Points a through f along the *y*-axis correspond to those in Figure 8.

regardless of whether or not ZAC shape was also modified (Fig. 9c,d,g,h). Similarly, models with posteriorly positioned ZACs in MH1 (Fig. 10,c,d,g,h) exhibit subtly lower strains than are observed in the unmodified model, with a few exceptions.

Results for the line transect data support those for the color mapping. Examination of von Mises strain magnitudes collected along the six facial transects reveal that differences between model variants are only very minor for some areas of the face, while others experience large differences in strain magnitudes. As a generalization, strain magnitudes were systematically higher in Sts 5 than MH1, and higher during premolar than molar loading, across all transects. Along Transect 1 (Fig. 11), which runs superiorly along the nasal margin, Sts 5 model variants exhibit only very minor differences in strain magnitude from the canine alveolus (point a) to just below the root of the nasal margin (point c). Large differences are found from the "nasal root" to the middle of the nasal margin, particularly between points c and d, for both LP^3 and LM^2 biting. In this region, Sts 5 model variants that include an anteriorly shifted zygomatic root complex (Sts 5 P-MOD, Sts 5 SP-MOD) exhibit elevated magnitudes of von Mises strain. In contrast, Sts 5 S-MOD was found to be very similar but slightly stronger in this region than Sts 5 UNMOD. This trend continues from point d until roughly mid-way to the intersection of Transect 1 and Transect 3 (point e). Here, the trend reverses from point e to point f, where Sts 5 P-MOD and Sts 5 SP-MOD experience lower strain magnitudes than Sts 5 UNMOD and Sts 5 S-MOD. With respect to the MH1 model variants, strains along the

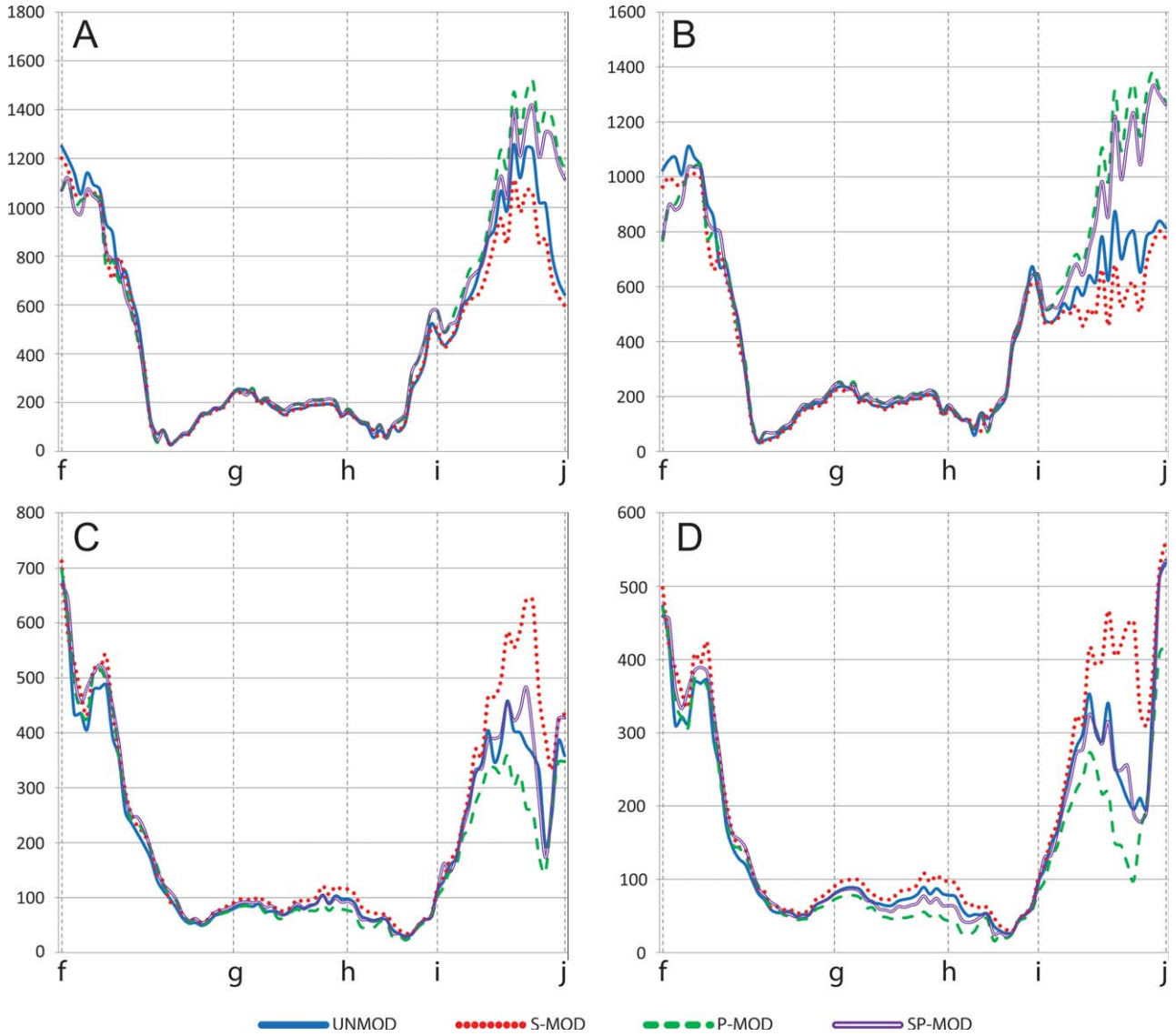

Fig. 12. Line graphs showing differences in the von Mises microstrain (*y*-axis) along Transect 2 between UNMOD, S-MOD, P-MOD, and SP-MOD variants of Sts 5 during (**A**) LP^3 and (**B**) LM^2 biting, and model variants of MH1 during (**C**) LP^3 and (**D**) LM^2 biting. Points f through j along the *x*-axis correspond to those in Figure 8.

nasal margin were also elevated to a subtle degree among variants that possessed an anteriorly positioned zygomatic root complex, at least during LP^3 biting. Differences between MH1 model variants were much smaller than in Sts 5, with the most pronounced differences being found just superior to the nasal root (point c) during LP^3 biting. During LM^2 biting, the largest differences are found further superiorly, along the upper half of the nasal margin (between points d and e). However, here the model variants with a ZAC modified to be more curved (MH1 S-MOD, MH1 SP-MOD) are those that experience the elevated strain magnitudes.

For the most part, von Mises strain magnitudes along Transect 2 (Fig. 12) are similar during LP^3 and LM^2 biting across model variants of both Sts 5 and MH1. However, postorbital bar (from points i to j) strains exhibit some large differences related to the zygomatic modifications. In both Sts 5 and MH1, model variants with an anteriorly positioned zygomatic root complex and a curved ZAC (Sts 5 P-MOD, MH1 S-MOD) experienced the highest strain magnitudes along the bar. Those that experienced the lowest postorbital bar strains were those with a posterior root complex coupled with a straight/steep ZAC (Sts 5 S-MOD and MH1 P-MOD). For Sts 5, there is a clear pattern where postorbital bar strains are highest among variants with an anteriorly placed zygomatic root complex (Sts 5 P-MOD and Sts 5 SP-MOD). This pattern is similar in MH1, particularly during, LM^2 biting, except that MH1 UNMOD never exclusively groups with MH1 S-MOD in this region.

Von Mises strain magnitudes along Transect 3 (Fig. 13), which extends from the superior aspect of the nasal

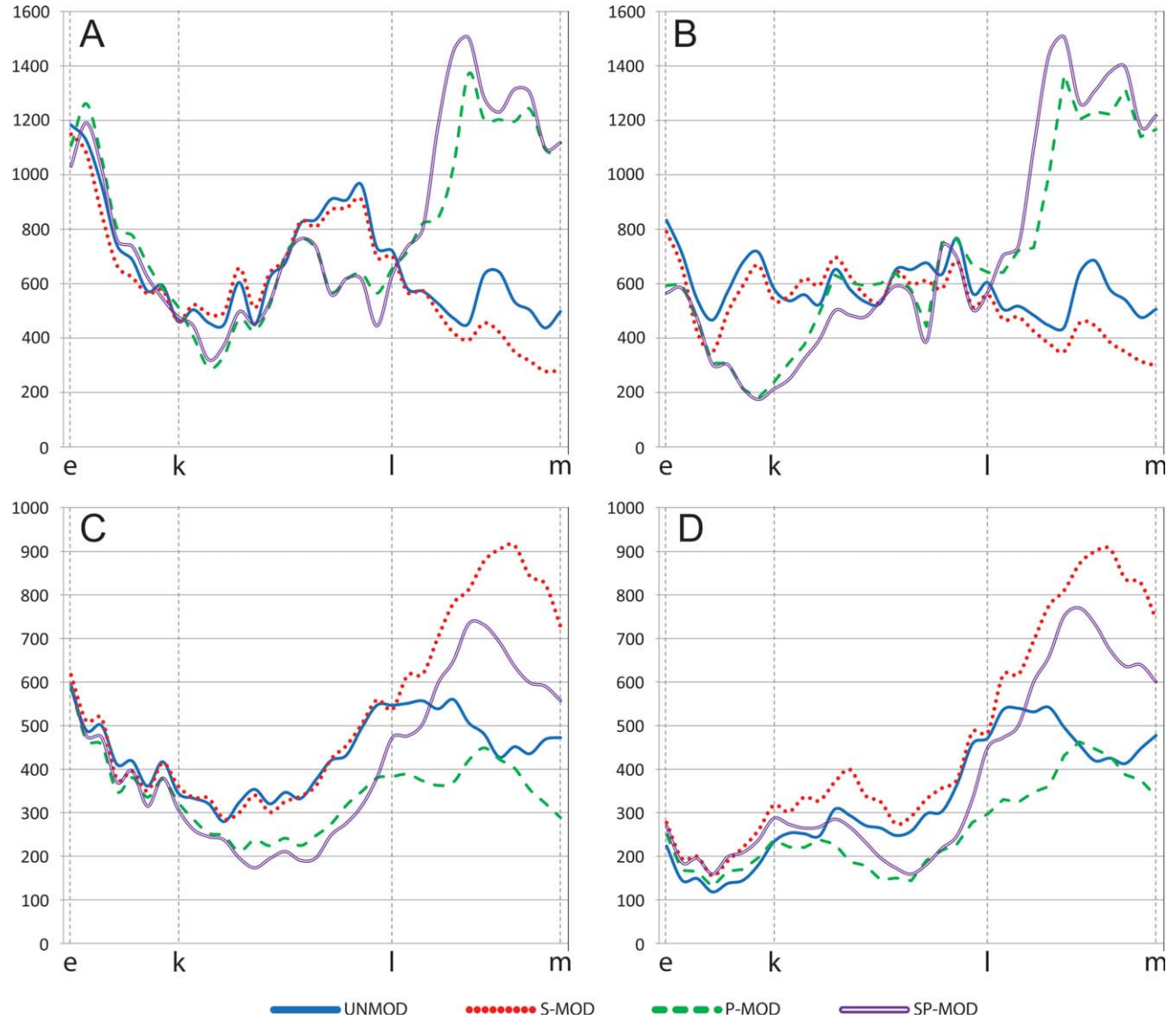

Fig. 13. Line graphs showing differences in the von Mises microstrain (*y*-axis) along Transect 3 between UNMOD, S-MOD, P-MOD, and SP-MOD variants of Sts 5 during (**A**) LP^3 and (**B**) LM^2 biting, and model variants of MH1 during (**C**) LP^3 and (**D**) LM^2 biting. Points e, k, l, and m along the *x*-axis correspond to those in Figure 8.

margin to the zygomatic protuberance (i.e., upper zygomatic body), were generally similar across model variants of both Sts 5 and MH1 along the segment that extends laterally across the superior aspect of the nasal margin (path e–k), although anterior positioning of the root complex does result in slightly elevated strains. More pronounced differences are seen along the infraorbital segment (path k–l) and particularly as the transect approaches the zygomatic protuberance (path l–m). In Sts 5, models with posteriorly-placed ZRCs (Sts 5 UNMOD, Sts 5 S-MOD) experience slightly elevated strain magnitudes along path k–l. This pattern is similar for both LP^3 and LM^2 biting, although during LM^2 biting there are larger differences along path e–k and smaller differences along path k–l. At the zygomatic protuberance (path l–m), the pattern reverses, and strains increase dramatically in models that have anteriorly-placed roots (Sts 5 SP-MOD, Sts 5 P-MOD). In MH1, however, models with an anteriorly-placed ZRC (MH1 UNMOD, MH1 S-MOD) generate the highest strains along the infraorbital segment of Transect 3, the opposite of what was observed among variants of Sts 5, but strains increase steeply as the transect moves laterally onto the zygomatic protuberance in the models that possess a curved ZAC (MH1 S-MOD, MH1 SP-MOD). Despite these differences, the models with the strongest zygomatic bodies (i.e., those that experience the lowest strain magnitudes) for both species were those that combined a posteriorly-positioned root complex and a straight/steep ZAC (Sts 5 S-MOD, MH1 P-MOD), for both LP^3 and LM^2 biting.

Along Transect 4, which passes from the mid-nasal margin region toward the middle of the ZAC, strains

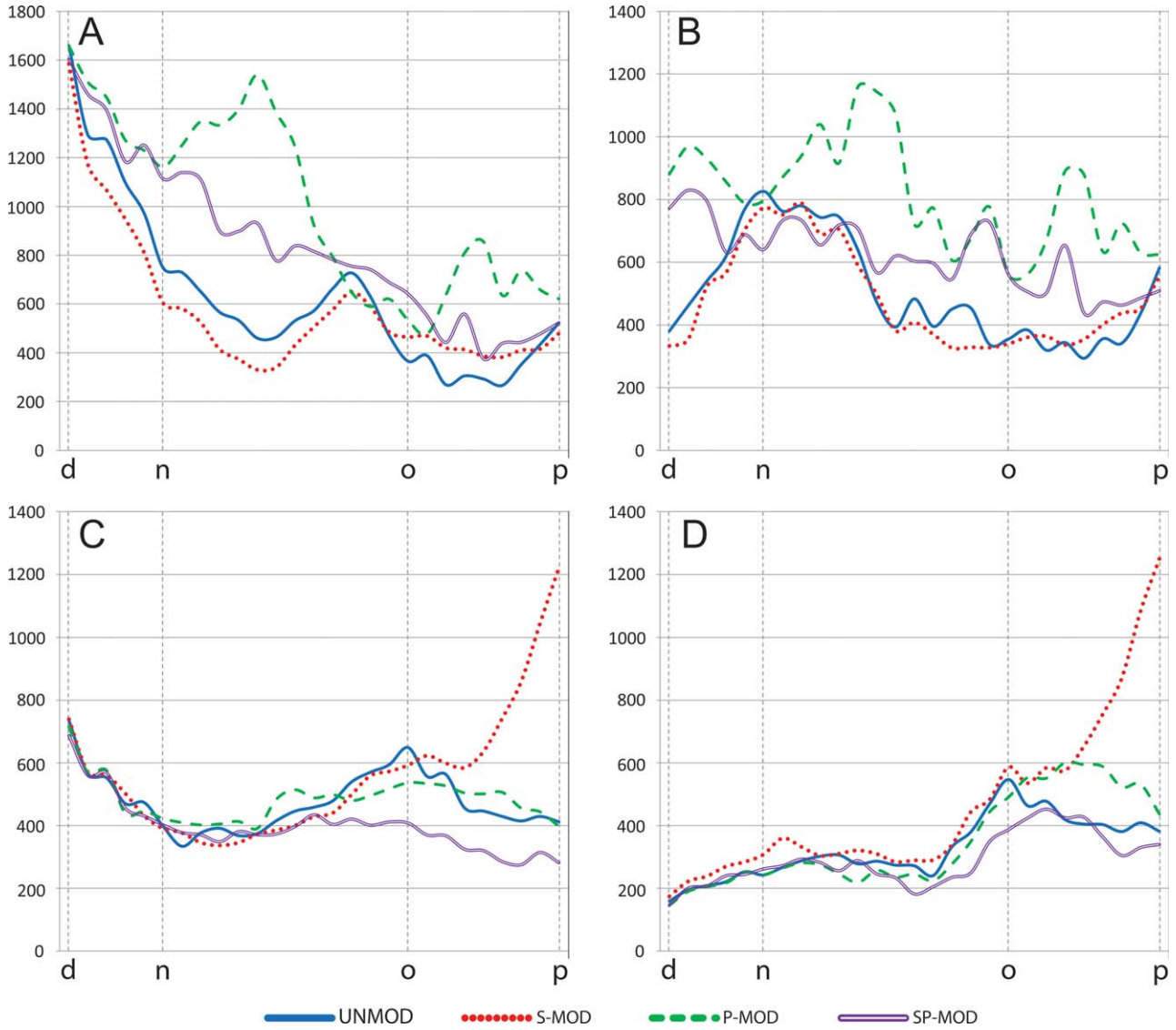

Fig. 14. Line graphs showing differences in the von Mises microstrain (*y*-axis) along Transect 4 between UNMOD, S-MOD, P-MOD, and SP-MOD variants of Sts 5 during (**A**) LP^3 and (**B**) LM^2 biting, and model variants of MH1 during (**C**) LP^3 and (**D**) LM^2 biting. Points d, n, o, and p along the *x*-axis correspond to those in Figure 8.

generated by Sts 5 model variants were generally highest among those with an anteriorly-positioned ZRC for both LP^3 and LM^2 biting (Fig. 14). In particular, the model exhibiting both an anteriorly-positioned root complex and curved ZAC (Sts 5 P-MOD) experienced highly elevated von Mises strain magnitudes along the infraorbital segment of Transect 4 (path n-o), as well as the anterior aspect of the zygomatic approaching the ZAC (path o-p). There were smaller and more variable differences along most of Transect 4 between model variants of MH1. However, similar to what was observed for Sts 5, the MH1 variant combining anterior positioning of the root and a curved ZAC (MH1 S-MOD) exhibited the most highly elevated strain magnitudes as the transect moves laterally between points o and p. This model was found to exhibit a much greater increase in strain over the other MH1 variants than between the variants of Sts 5.

Transect 5 extends from the nasal aperture to the root of the zygomatic where it meets the maxilla. In both Sts 5 and MH1, strains are highest during LP^3 biting among model variants that possess an anteriorly-positioned ZRC along the majority of the transect (Fig. 15), whether the zygomatic is curved or straight/steep (Sts 5 P-MOD, Sts 5 SP-MOD; MH1 S-MOD, MH1 UNMOD). However, in both species, strains approaching the zygomatic root (path s-t) generate the highest von Mises strain magnitudes among variants with a curved ZAC, whether the zygomatic root complex is anteriorly or posteriorly placed (Sts 5 P-MOD, Sts 5 UNMOD; MH1 S-MOD, MH1 SP-MOD). Additionally, as Transect 5 approaches the zygomatic root (point t), both species

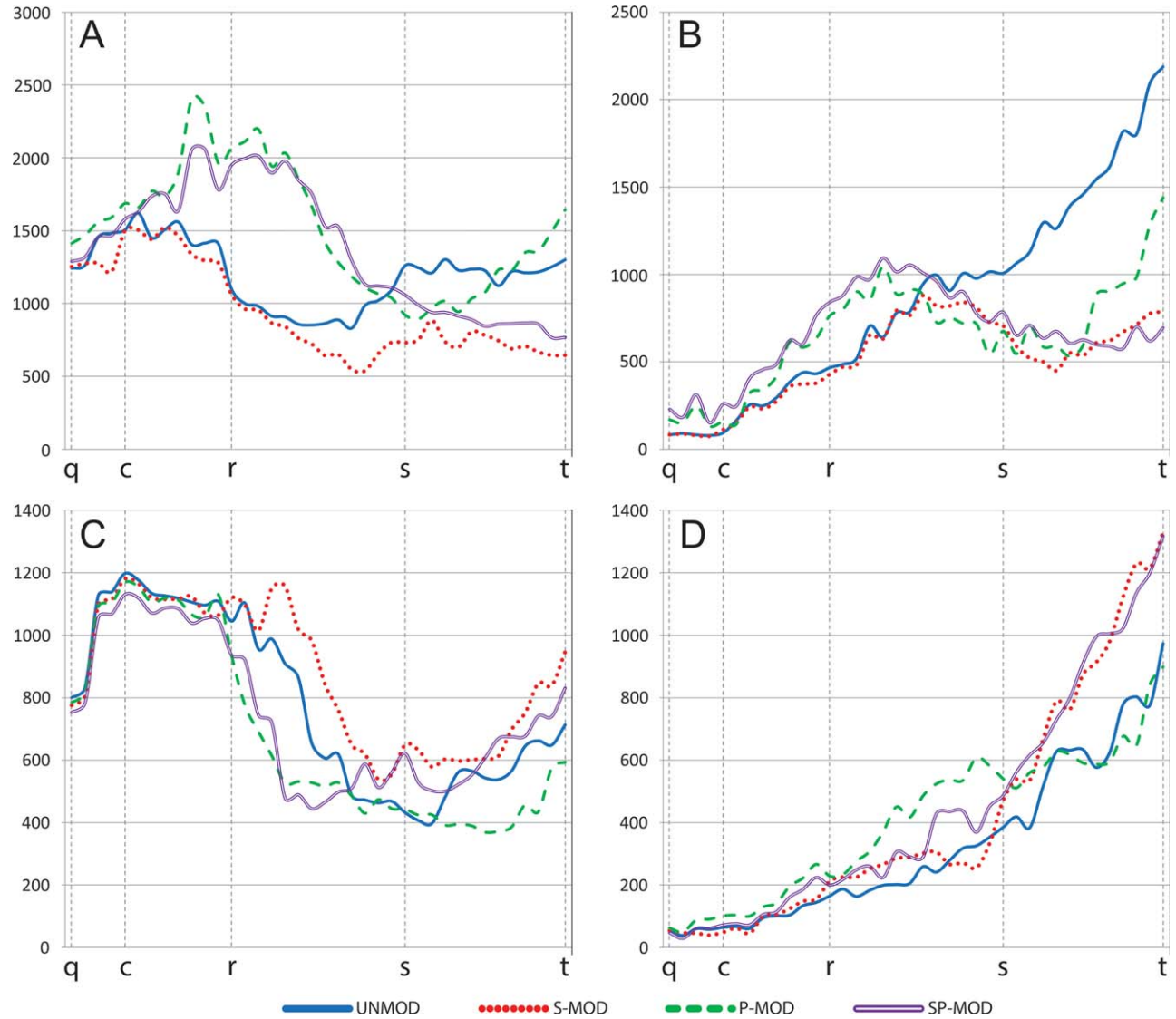

Fig. 15. Line graphs showing differences in the von Mises microstrain (*y*-axis) along Transect 5 between UNMOD, S-MOD, P-MOD, and SP-MOD variants of Sts 5 during (**A**) LP^3 and (**B**) LM^2 biting, and model variants of MH1 during (**C**) LP^3 and (**D**) LM^2 biting. Points q, c, r, s, and t along the *x*-axis correspond to those in Figure 8.

exhibit a pattern where the magnitude of von Mises strain is greatest during LP^3 biting among model variants that exhibit an anterior/curved morphology (Sts 5 P-MOD, MH1 S-MOD), followed by posterior/curved (Sts 5 UNMOD, MH1 SP-MOD) and anterior/straight (Sts 5 SP-MOD, MH1 UNMOD) morphologies, with the lowest zygomatic root strains experienced by those with a posterior/straight morphology (Sts 5 S-MOD, MH1 P-MOD). The pattern for LM^2 biting is generally similar to that observed for LP^3 biting in both species, with curved ZACs experiencing the most elevated strain magnitudes between point s and t, although the pattern is more variable between points q and s.

Transect 6 wraps around the anterior rostrum, terminating near a point just distal to the LM^2 alveolus. Sts 5 and MH1 model variants exhibit only minor differences in von Mises strain magnitudes as the transect moves distally toward point v, which lies just above LP^3 (Fig. 16). During LP^3 biting, this point generated the highest magnitudes of strain no matter the model variant. From points v to x, the differences between model variants of Sts 5 and those of MH1 were somewhat greater but also highly variable. However, Sts 5 model variants with anterior roots (Sts 5 P-MOD, Sts 5 SP-MOD) show a pattern of higher strains along the first half of the v–x segment, but lower strains along its distal half. For LM^2 loading, the highest strain magnitudes are generated above the loaded tooth (point w) in most models. However, those with anterior roots (Sts 5 P-MOD, Sts 5 SP-MOD; MH1 UNMOD, MH1 S-MOD) experience peak strain magnitude mesial to LM^2, particularly among variants of MH1. In Sts 5 and MH1, models with anteriorly

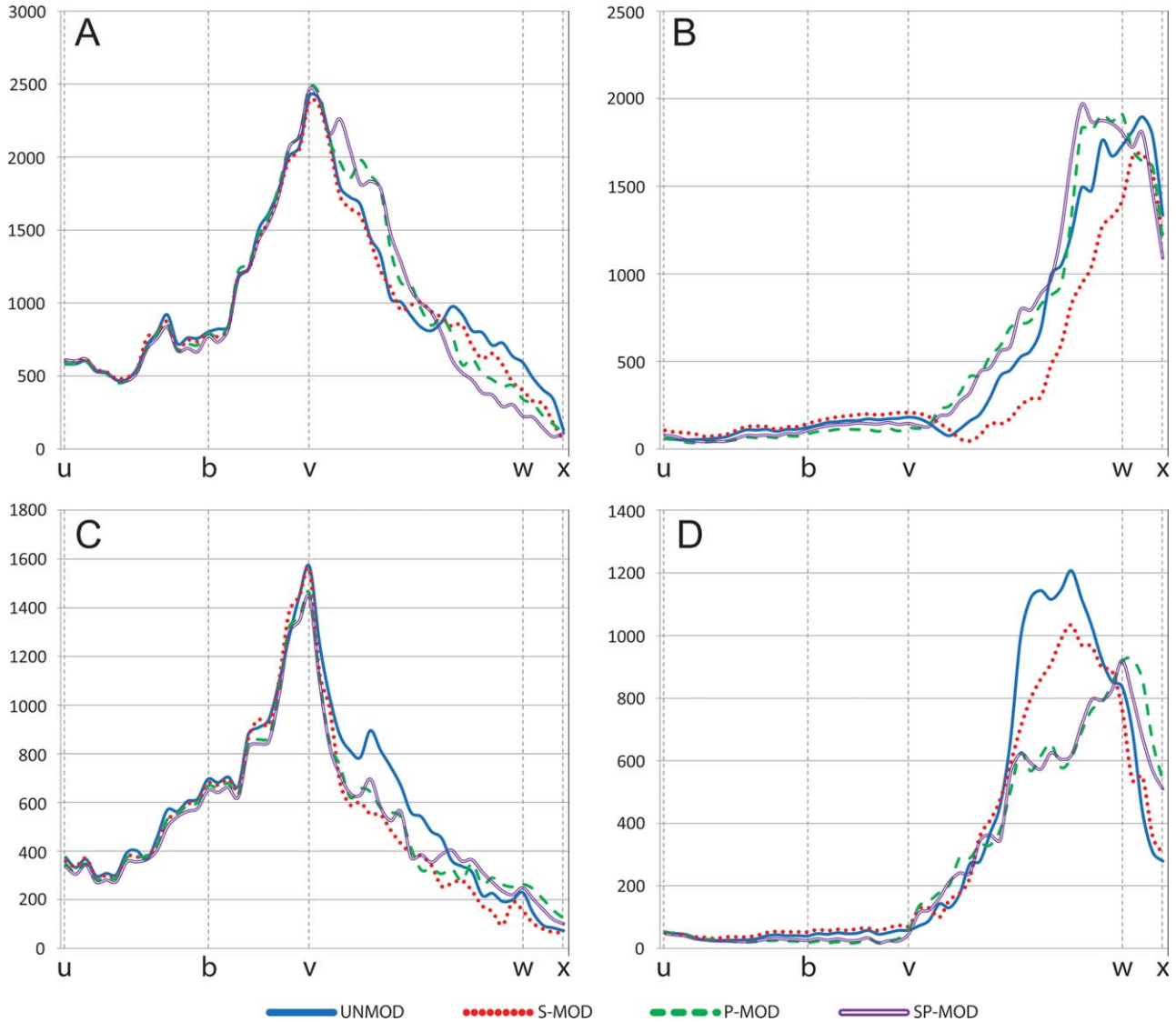

Fig. 16. Line graphs showing differences in the von Mises microstrain (*y*-axis) along Transect 6 between UNMOD, S-MOD, P-MOD, and SP-MOD variants of Sts 5 during (**A**) LP^3 and (**B**) LM^2 biting, and model variants of MH1 during (**C**) LP^3 and (**D**) LM^2 biting. Points u, b, v, w, and x along the *x*-axis correspond to those in Figure 8.

placed roots also experience generally higher strain magnitudes as the transect moves toward the LM^2 bite point from LP^3 (path v–x).

In addition to the data on von Mises strain magnitudes presented above, bite forces, biting efficiency (i.e., mechanical advantage), and temporomandibular (TMJ) reaction forces were recorded from all model variants and compared (Table 2). These data reveal that models with anteriorly positioned zygomatic roots (Sts 5 P-MOD, Sts 5 SP-MOD; MH1 UNMOD, MH1 S-MOD), and thus a more anteriorly positioned superficial masseter origin, generate bite forces with greater efficiency (i.e., higher mechanical advantage) than model variants with posteriorly positioned roots. Each set of model variants were assigned the same muscle force magnitudes, but this increase in efficiency resulted in bite forces that were greater in models with an anteriorly placed ZRC than those with posteriorly placed ZRCs, in addition to the observed increase in strain noted above. Additionally, a forward shift of the zygomatic in Sts 5 (Sts 5 P-MOD, Sts 5 SP-MOD) resulted in working-side TMJ distraction (tension) during molar biting, which was not observed for Sts 5 UNMOD. Similarly, MH1 model variants with posteriorly shifted roots (MH1 P-MOD, MH1 SP-MOD) generate distractive forces during molar biting that were lower in magnitude than the unmodified original (see also Ledogar et al., 2016a). These reaction force data are fully consistent with predictions of the constrained lever model of jaw biomechanics (Greaves, 1978; Spencer, 1999).

TABLE 2. Muscle force input, bite force output, mechanical advantage (MA) of biting, and reaction forces at the working-side (WS) and balancing-side (BS) temporomandibular joints (TMJ) during premolar (LP^3) and molar (LM^2) biting for the UNMOD, S-MOD, P-MOD, and SP-MOD variants of Sts 5 and MH1

		UNMOD	S-MOD	P-MOD	SP-MOD
Sts 5	Input muscle force[a]	2893	2893	2893	2893
	LP^3 bite force	1178	1177	1235	1251
	LP^3 MA	0.41	0.41	0.43	0.43
	LM^2 bite force	1786	1784	1872	1897
	LM^2 MA	0.62	0.62	0.65	0.66
	WS TMJ reaction - LP^3	454.78	459.91	410.72	391.5
	BS TMJ reaction - LP^3	842.5	837.68	814.42	794.97
	WS TMJ reaction - LM^2	48.44	52.2	−2.46	−38.26
	BS TMJ reaction - LM^2	685.73	682.41	664.12	634.43
MH1	Input muscle force[a]	2658	2658	2658	2658
	LP^3 bite force	1043	1022	970	953
	LP^3 MA	0.39	0.38	0.36	0.36
	LM^2 bite force	1827	1790	1699	1669
	LM^2 MA	0.69	0.67	0.64	0.63
	WS TMJ reaction - LP^3	310.68	328.6	363.78	375.69
	BS TMJ reaction - LP^3	845.63	857.35	871.78	875.19
	WS TMJ reaction - LM^2	−154.81	−140.12	−101.3	−87.95
	BS TMJ reaction - LM^2	624.78	635.02	641.78	641.38

[a]Bilaterally symmetrical muscle forces.
[b]Bite and TMJ reaction forces are in Newtons (N). Positive values indicate compression, whereas negative values indicate tension (distraction).

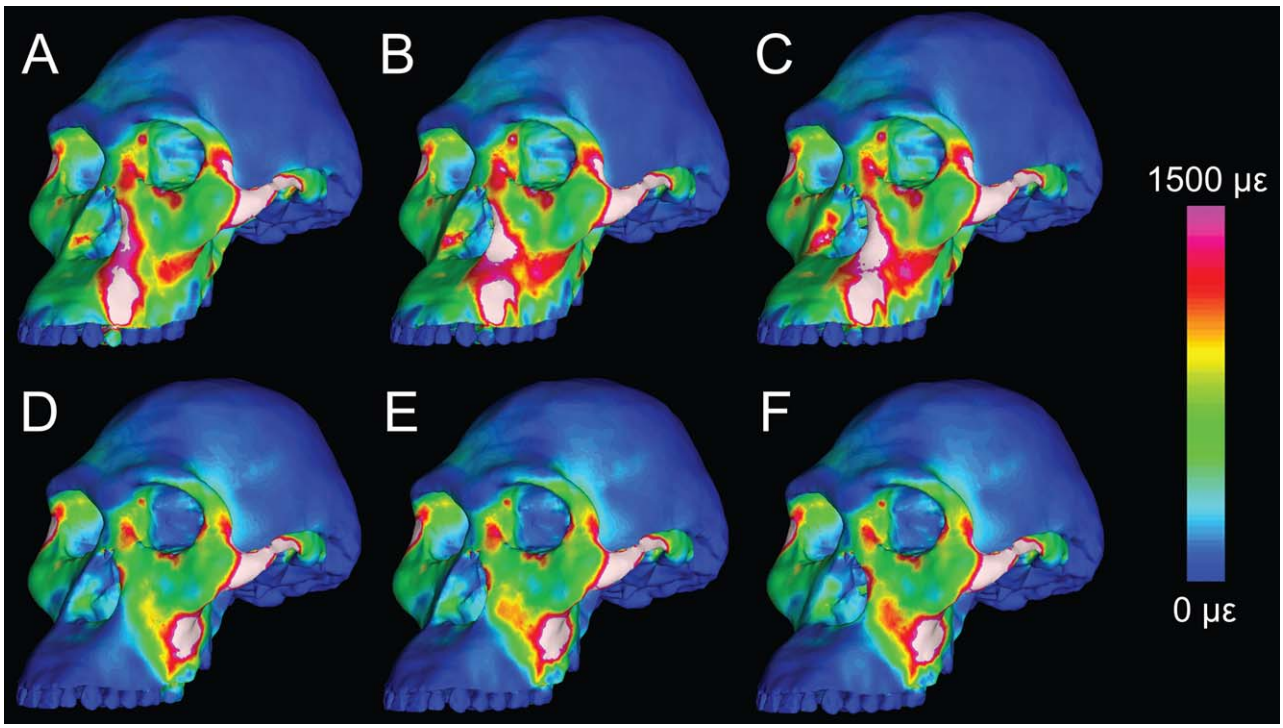

Fig. 17. FEMs of Sts 5 UNMOD (**A**, **D**), Sts 5 NP-1 (**B**, **E**), and Sts 5 NP-2 (**C**, **F**) showing the increase in von Mises strain magnitude following the "removal" of the anterior pillars. The top row shows strains generated during LP^3 biting, while the bottom row shows LM^2 biting. The von Mises strain is shown at a scale of 0 to 1500 με. White regions exceed scale.

The Anterior Pillars

Color mapping of von Mises strains generated by the unmodified model of Sts 5 (Sts 5 UNMOD) compared to those generated by the two "No-Pillar" variants (Sts 5 NP-1, Sts 5 NP-2) reveals that the digital "removal" of the anterior pillars in FEMs of *A. africanus* (Sts 5) significantly increases strain magnitudes generated during simulations of occlusal loading (Fig. 17). Strain

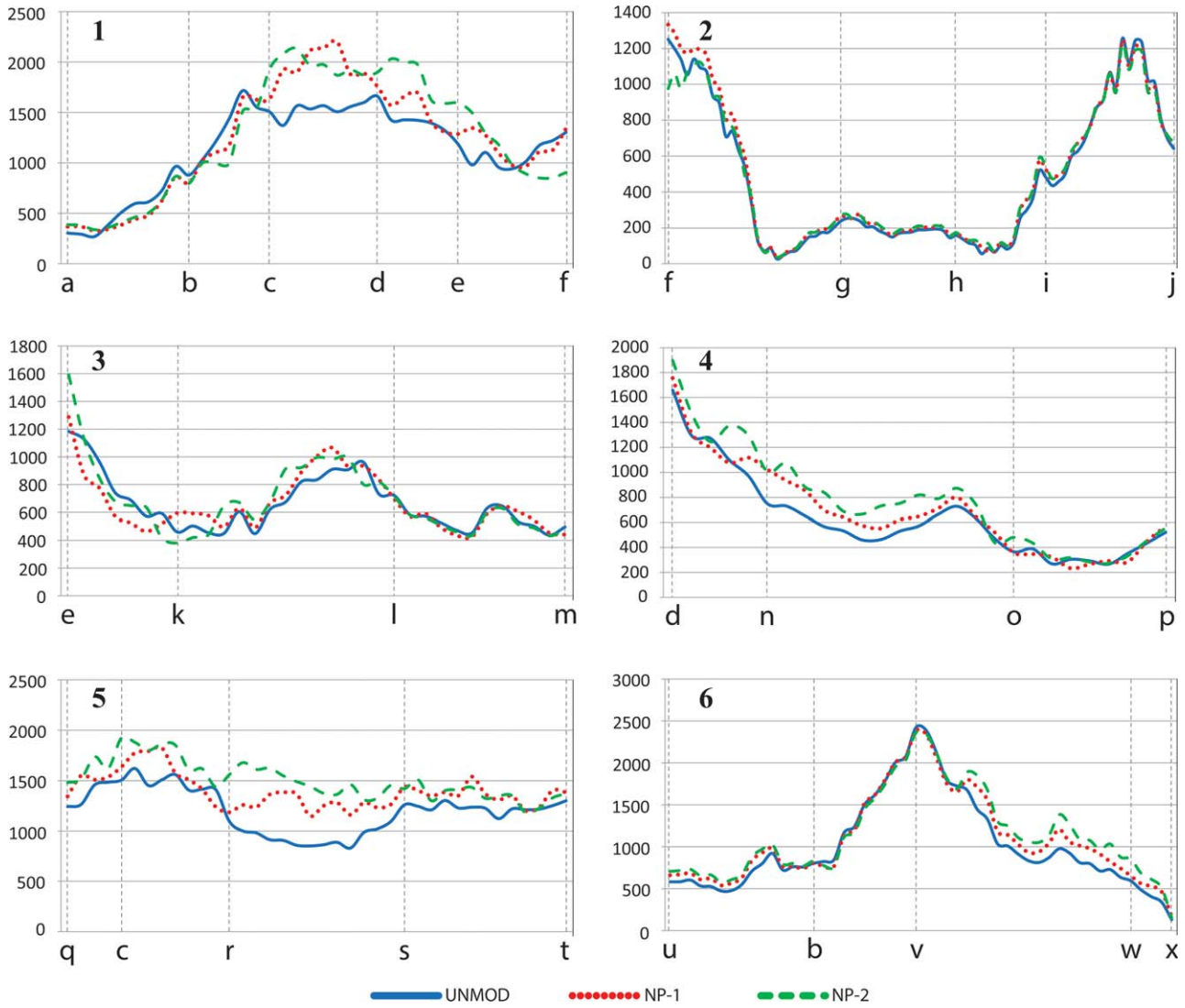

Fig. 18. The von Mises microstrain (*y*-axis) generated during LP^3 biting along each of the six line transects in FEMs of Sts 5 UNMOD and the two "No-Pillar" model variants, Sts 5 NP-1 and Sts 5 NP-2. Points along each *x*-axis correspond to Figure 8.

magnitudes were typically higher during premolar than molar loading. Although differences can be found across many parts of the facial skeleton, the most conspicuous variation in strain magnitudes between model variants occur along the nasal margin itself (Transect 1) and at the inferior portion of the infraorbital plate near the junction of the zygomatic and lower portion of the rostrum (Transect 5).

Data on von Mises strain magnitudes collected from finite elements lying along six facial transects (Figs. 18 and 19) further demonstrate that large increases are found along the nasal margin (Transect 1) in the Sts 5 NP-1 and NP-2 model variants. The largest increases are experienced along the inferior to middle portion of the margin (path c–d). For example, Sts 5 NP-1 is subjected to von Mises strain magnitudes over one third higher than the unmodified model during LP^3 biting as a result of simply flattening the pillar. Except for the superior portion (Transect 3, e–k), elements that span laterally across the pillar region (Transect 4, d–n; Transect 5, c–r) also exhibit moderate to large differences. The "No-Pillar" models experience even larger increases in strain magnitude near the inferior portion of the infraorbital plate during LP^3 biting. In particular, strain magnitudes in Sts 5 NP-2 experienced highly elevated von Mises strain magnitudes along Transect 5 as it approaches the zygomatic root (path r–s). Smaller but notable increases occur at the root (path s–t), as well as and along Transect 4 between points n and o. In contrast, circumorbital (i.e., interorbital, supraorbital, and postorbital bar) strains collected from finite elements that follow Transect 2 did not vary all that much between the model variants, with the only notable differences at the interorbital, near the most superior aspect of the nasal margin. However, here, as with the superior nasal

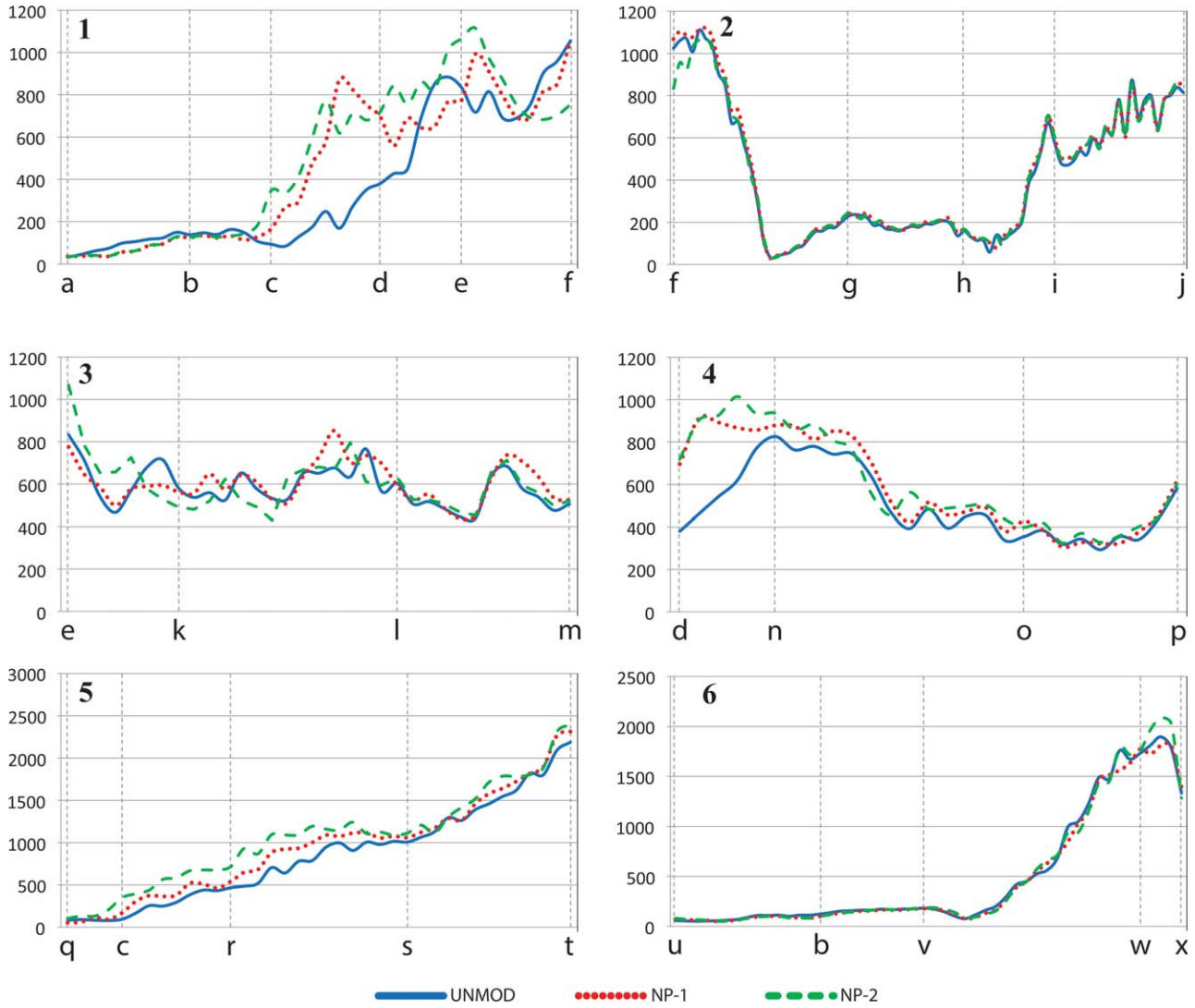

Fig. 19. The von Mises microstrain (*y*-axis) generated during LM^2 biting along each of the six line transects in FEMs of Sts 5 UNMOD and the two "No-Pillar" model variants, Sts 5 NP-1 and Sts 5 NP-2. Points along each *x*-axis correspond to Figure 8.

margin, strain magnitudes were found to be slightly lower in Sts 5 NP-2 than in the other two models. Most of Transects 3 and 6 also did not vary greatly between the model variants. However, during LP^3 biting, slight differences in strain can be seen along the anterior rostrum (Transect 6, u–b), in addition to some more moderate differences along the lateral maxilla (Transect 6, v–x), with No-Pillar models experiencing larger strain magnitudes in both cases. In general, the pattern of differences between the original and "No Pillar" models during LP^3 biting were also observed for the LM^2, but with differences being generally less pronounced and more variable in the latter. However, the medial portion of the nasal margin (Transect 1, c–d; Transect 4, d–n), which normally experiences low strain magnitudes, was subjected to proportionally larger increases in strain magnitude as a result of the pillar modifications.

DISCUSSION

We examined variants of our previously constructed finite element models (FEMs) of *A. africanus* (Sts 5; Smith et al., 2015a) and *A. sediba* (MH1; Ledogar et al., 2016a) in order to test hypotheses related to the mechanical role of bony features purported to strengthen the face during feeding. These included our unmodified originals (UNMOD) and three variants per species that were modified to differ in the morphology of the zygomaticoalveolar crest (ZAC) and zygomatic root complex (ZRC), including its shape (S-MOD), position (P-MOD), or both shape and position (SP-MOD). These resulted in variants that had either: a curved ZAC and posteriorly positioned ZRC (Sts 5 UNMOD, MH1 SP-MOD), a curved ZAC and anteriorly positioned ZRC (Sts 5 P-MOD, MH1 S-MOD), a straight/steep ZAC and posteriorly positioned ZRC (Sts 5 S-MOD, MH1 P-MOD), or a

straight/steep ZAC and anteriorly placed ZRC (Sts 5 SP-MOD, MH1 UNMOD). Many of these combinations are found among living primates and in fossils hominins. For example, a curved/posterior morphology is found in *A. afarensis* and at least one *A. africanus* specimen (Sts 5). Chimpanzees and gorillas have more posteriorly positioned ZRCs than in the australopiths and also have curved ZACs (some are straight and therefore more similar to the straight/posterior variants). A curved ZAC is thought to be the plesiomorphic condition (see Kimbel et al., 2004), and is also present in *Homo*, which exhibits the curved/anterior condition. The straight/anterior condition seen in MH1 is found among most other *A. africanus* specimens, and is taken to extreme levels in the robust australopiths. However, because MH1 and Sts 5 differ morphologically in a number of other respects, including differences in facial prognathism (Berger et al., 2010; see below), these combinations resulted in some hypothetical morphologies not necessarily present in known species. These models serve an important comparative purpose. For example, because Sts 5 exhibits high levels of facial prognathism, anterior positioning (Sts 5 P-MOD) results in somewhat of a hypothetical configuration. However, with the addition of a straight/steep ZAC (Sts 5 SP-MOD), it resembles the "visor" found among robust australopiths, especially prognathic specimens like KNM-WT 17000. Comparisons involving Sts 5 P-MOD are therefore useful when evaluating Rak's (1983) predictions concerning "visorlike" zygomatic morphology in *Paranthropus* (see below).

Hypothesis 1: Zygomatic Morphology and Mechanical Variation

We found that the presence of a straight and steep ZAC structurally reinforces the face, reducing stresses from both bite and muscle forces during feeding. These findings support Rak's (1983) hypothesis that a straight/steep ZAC strengthens the face against feeding loads. For some regions of the face, strains were over 200% lower in model variants with straight/steep crests compared to the unmodified originals. However, structural modifications to the zygomatics of MH1 and Sts 5 were not found to result in *globally* increased or decreased craniofacial strain magnitudes. Instead, by examining strains along the six line transects, which each capture variation across various facial regions, the mechanical consequences of the modifications were found to follow regional responses to variation in facial structure. Areas of the face that were the most impacted by changes in zygomatic shape were confined mainly to the zygomatic region itself, in particular the lateral infraorbital/zygomatic plate region of MH1, near the junction of the zygomatic arch and zygomatic root (Transect 4, o–p). Unlike in Sts 5, MH1 S-MOD experienced an increase in von Mises strain magnitude over 200% (up to ~870 με) during LM^2 biting, and saw similar increases during LP^3 biting (see Fig. 14). These represent the largest differences in strain magnitude between an unmodified FEM and an S-MOD variant. Therefore, this region may have been particularly susceptible to high strain magnitudes in *A. sediba*, which might help explain the retention of a straight/steep ZAC despite an overall reduction in facial size and robusticity.

Other regions that experienced large proportional differences as a result of the shape modifications include the inferior postorbital bar, zygomatic body, and zygomatic root. For example, near the end of the postorbital bar transect (Transect 2, i–j), MH1 S-MOD experienced strain magnitudes that were as high as ~130% (>250 με) greater than MH1 UNMOD during LM^2 biting, and nearly 80% (~280 με) greater during LP^3 biting (see Fig. 12). Differences in this region were less pronounced when comparing Sts 5 UNMOD with Sts 5 S-MOD, reaching a maximum increase of 22% (195 με) during LM^2 biting. Similarly, at the zygomatic body (Transect 3, l–m), strain magnitudes were increased by over 110% (~480 με) in MH1 S-MOD during both LP^3 and LM^2 biting, with a decrease of smaller magnitude (~35%, 230 με) likewise experienced along this segment in Sts 5 S-MOD (see Fig. 13). Sts 5 and MH1 responded similarly to the shape modifications along Transect 5, which extends from the inferior corner of the nasal margin to the zygomatic root. During LM^2 biting, Sts 5 S-MOD experienced a decrease in strain magnitudes of ~60% (~900 με) across the r–s segment of Transect 5, while MH1 S-MOS similarly experienced up to a 56% (~440 με) decrease in strain near the lateral end of this segment (see Fig. 15). Differences between models were slightly less pronounced here during LP^3 biting (~50% in both specimens), with the bite point being positioned further from the root.

In contrast to the results for ZAC shape, anterior positioning of the zygomatic root was found to increase, rather than decrease, facial strain magnitudes for many regions, even in models that also possessed a straight/steep ZAC. In fact, changes in zygomatic positioning were often found to produce the largest differences in strain magnitudes, particularly among model variants of Sts 5. For example, the zygomatic body/zygomatic protuberance (Transect 3, l–m) of the P-MOD and SP-MOD variants of Sts 5 experienced huge increases (>200%) in von Mises strain magnitudes during both LP^3 and LM^2 biting (see Fig. 13). The same is true for variants of MH1, but with a more even-balanced distribution. However, in models that exhibit an anteriorly placed zygomatic root complex, lower strain magnitudes in general were observed for those that combined a straight/steep ZAC.

It is conceivable that the stronger effect of root position in Sts 5 than MH1 relates to overall levels of facial prognathism, which is greater in Sts 5 than in MH1. The mesognathic facial profile of MH1 (Berger et al., 2010) appears to be the result of a higher degree of facial retraction, as opposed to an anterior migration of the zygomatic, as in *Paranthropus* (Smith et al., 2015b). Three indices that express the relative position of the palate in early hominins were measured in Rak's (1983) analysis of the australopithecine face. Of these, the proportion of the palate's protrusion anterior to sellion is the only that does not include masticatory landmarks (i.e., zygomatic root, articular eminence). We quantified this index in the unmodified models of MH1 and Sts 5 using total palate length (as opposed to dental arcade length, because the third molars of MH1 are unerupted). Our unmodified model of Sts 5 has an index of 0.67, which is very close to the value of 0.68 measured from the fossil by Rak (1983) using dental arcade length. We calculated a value of 0.47 from our model of MH1, which

has a much greater proportion of its palate tucked beneath the upper portion of the face. This plays an important role in several aspects of feeding biomechanics in MH1, including biting efficiency and the generation of distractive reaction forces at the jaw joint during forceful molar biting (Ledogar et al., 2016a). Additionally, facial retraction (as opposed to anterior migration of the zygomatic) might, in some cases, have a strengthening effect (but see Ledogar et al., 2016b).

Overall, the results for the comparisons between the UNMOD and P-MOD FEMs contrasts with the predictions presented above. Rak (1983) predicted that both the shape of the zygomatic root and its position relative to the dental arcade played key roles in early hominin feeding biomechanics. Likewise, other workers have suggested that more anteriorly positioned zygomatics, and thus more orthognathic facial profiles, reduce bending moments in the face among modern humans that engage in extensive anterior dental loading (e.g., Inuit [Hylander, 1977]). However, because an anterior migration of the zygomatic root complex also increases the mechanical advantage (i.e., leverage) of the superficial masseter muscle, the corresponding increase in bite force was instead found here to increase strain magnitudes for many facial regions. Therefore, although Rak (1983) also notes the importance of zygomatic root positioning to the production of bite force, his prediction that it also reduces rostral bending is not supported by the results presented here.

Although anterior positioning was generally found to increase strains, certain regions experienced slightly lower magnitudes with the addition of an anterior root complex. For example, in both Sts 5 and MH1, models with an anteriorly positioned root complex experienced the highest strain magnitudes near the root of the nasal margin (Transect 1, c–d), but the lowest near its more superior portion (e–f). Additionally, despite this "common pattern" observed for MH1 and Sts 5 (i.e., straight/steep ZAC decreasing strain, anteriorly positioned zygomatic root complex increasing strain), they sometimes followed an opposite pattern. For example, anterior positioning of the zygomatic root in MH1, as in MH1 UNMOD and MH1 S-MOD, generates higher strain in the infraorbital region than MH1 models with posteriorly positioned roots (MH1 P-MOD, MH1 SP-MOD). The opposite of this pattern is observed in Sts 5. Pulling the zygomatic forward on the prognathic face of Sts 5 creates a "dish" in the infraorbital region, reminiscent of *Paranthropus*, where strain magnitudes are reduced (see Fig. 9). For example, during LP^3 biting, anterior positioning of the root complex in Sts 5 (i.e., Sts 5 P-MOD, Sts 5 SP-MOD) was found to increase strain magnitudes along the medial (path e–k) and lateral (path l–m) segments of Transect 3 but decrease strains along its infraorbital portion (k–l) (see Fig. 13). Even without this modification, the "zygomatic prominence" (Rak, 1983) of *A. africanus* creates a small infraorbital depression that is not found in the face of some other gracile australopiths, including *A. afarensis* (Kimbel et al., 2004).

Rak (1983) and Kimbel et al. (2004) note that, in robust australopiths, the anterior migration of the ZRC (along with the superficial masseter origin) relative to the orbital plane causes the infraorbital region to no longer act as a self-supporting structure, especially in more prognathic specimens (e.g., KNM-WT 17000). According to them, this necessitates architectural modifications to strengthen areas susceptible to high strain magnitudes, including the zygomatic root. In *Paranthropus* (and *Theropithecus brumpti* [Rak, 1983]), the enlarged and inflated zygomatic/infraorbital plate, combined with its anterior placement, results in a "visorlike" form. Likewise, in our model of Sts 5, one of the most prognathic of all australopith crania (Kimbel et al., 2004), anterior placement of the ZRC (i.e., Sts 5 P-MOD, Sts 5 SP-MOD) resulted in a facial configuration similar to the "visor" in *Paranthropus*. These models experienced elevated strain magnitudes that are unlikely to be caused by increases in leverage and bite force alone; an anteriorly placed zygomatic root weakens rather than strengthens the face, *contra* Rak (1983). However, our results are consistent with the predictions of Rak (1983) insofar as comparisons between Sts 5 P-MOD and Sts 5 SP-MOD show that when the root is anteriorly placed, the presence of an inflated zygomatic with a straight ZAC reduces strains. These reductions are particularly evident at the mid-infraorbital plate (Transect 4, n–o) and zygomatic root (Transect 5, s–t). Additional structural modifications would be required to reduce strains to levels seen in the unmodified model.

Hypotheses 2 and 3: The Anterior Pillars and Craniofacial Strength

With respect to the anterior pillars (AP), results of the analyses involving the "removal" of the pillars in FEMs of Sts 5 are consistent with Hypothesis 2, which states that the pillars function as a strut to resist high loads associated with premolar-focused biting on resistant foods in *A. africanus* (Rak, 1983; Strait et al., 2009). Results are also consistent with Hypothesis 3, which states that pillars serve as a general reinforcement that strengthens the face during molar loading. However, the nature of that reinforcement, as revealed by orientation of principal strains (see below), differs during premolar versus molar loading. The two "No-Pillar" variants, one with the pillar flattened, preserving the lateral facial profile (Sts 5 NP-1), and one with the anterior outpocketing of the maxillary sinus greatly reduced (Sts 5 NP-2), both generated highly elevated strain magnitudes along most of the nasal margin and at the zygomatic root. In particular, during LP^3 biting, the middle portion of the anterior pillar (Transect 1, just superior to point c) in Sts 5 NP-2 experienced von Mises strains that were on average one third higher, but at some points up to 50% ($\sim$700 $\mu\epsilon$) higher, than the unmodified FEM of Sts 5 (see Fig. 18). The lower to middle portion of the pillar (between points c and d) in Sts 5 NP-1 experienced similar increases simply as a result of flattening the pillar. Strains were also found to increase along the nasal margin during LM^2 biting. In particular, as with the premolar results, bites at the LM^2 generated strains that were up to $\sim$700 $\mu\epsilon$ higher along the c–d path of Transect 1 in the NP-1 model variant. However, because strains are normally relatively low here during molar biting, this difference amounts to a much larger proportional increase of over 400%.

During LP^3 biting, and somewhat during LM^2 biting, the "No-Pillar" Sts 5 model variants also experienced large increases in von Mises strain magnitude along Transect 5, particularly between points r and s

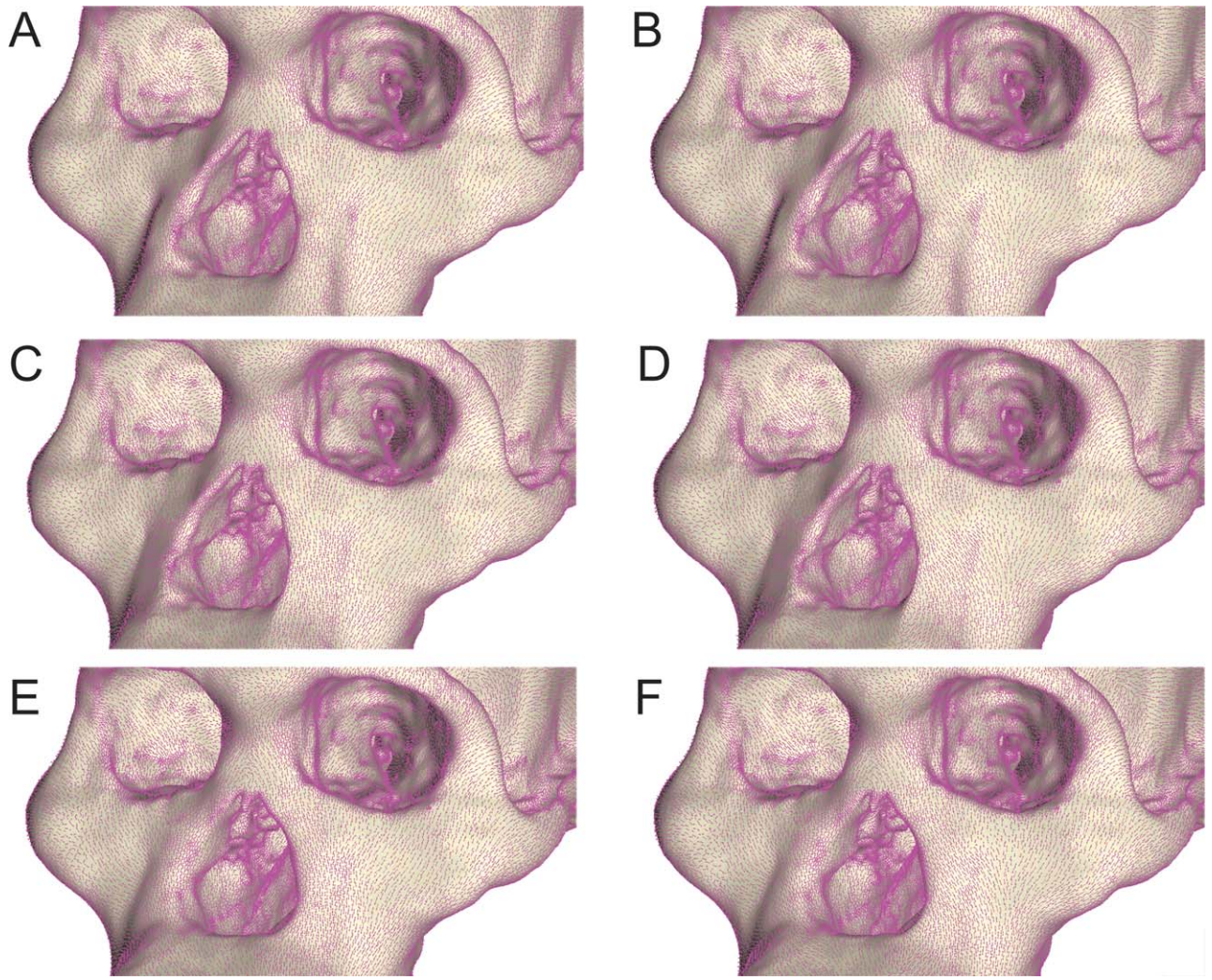

Fig. 20. Orientation of compressive strains during LP^3 (left column) and LM^2 (right column) biting in Sts 5 UNMOD (**A**, **B**), Sts 5 NP-1 (**C**, **D**), and Sts 5 NP-2 (**E**, **F**).

(see Fig. 18). This region, near the junction of the zygomatic and lower portion of the rostrum, which is commonly involved in facial fractures among humans (Ellis et al., 1985), experiences high strain magnitudes through the combination of its proximity to both the masseter muscle force and the premolar bite force. Relative to Sts 5 UNMOD, LP^3 biting generates von Mises strain magnitudes that reach increases of nearly 80% (~700 με) in the NP-2 variant, and nearly 60% (~500 με) higher in NP-1. Slightly smaller differences are observed during LM^2 biting for both NP-1 (~70%, 450 με) and NP-2 (~45%, 280 με). Therefore, because the "removal" of the pillars evidently increases strain in the anterior zygoma, particularly during premolar biting, selection for reducing masticatory stresses in this region may have also been a factor in the evolution of anterior pillars.

Although "removing" the pillar in Sts 5 causes a spike in strain along the nasal margin, this region is still quite weak compared to other parts of the face or even in comparison with other species. In fact, even with the large pillars of Sts 5 UNMOD, this model was found to experience strain magnitudes at the working-side pillar that exceeded those recorded for chimpanzees (Smith et al., 2015a). The fact that the anterior pillar of Sts 5 experiences such high strain magnitudes has been used as an argument against the hypothesis that it is selectively important for resisting large occlusal loads (Grine et al., 2010; Daegling et al., 2013). However, as discussed above, and as noted by previous authors (Strait et al., 2013; Ross and Iriarte-Diaz, 2014; Smith et al., 2015a), the anterior pillars of *A. africanus* and other regions of the face that experience elevated strain magnitudes (e.g., the zygomatic root) might reasonably be expected to respond to selection on their shape and size more so than areas that experience relatively low strain magnitudes, such as the brow ridges. Therefore, because the nasal margin of *A. africanus* (or at least represented by Sts 5) is apparently weak despite the presence of large pillars, our findings that the anterior pillars do in

fact lessen the particularly large strains this region is subjected to, especially during premolar biting, are consistent with Rak's (1983) hypothesis.

Strain orientation along the nasal margin of Sts 5 model variants (Fig. 20) may provide clues as to the selection pressures driving the evolution of the pillar in australopiths. Strain orientation data suggest that during premolar biting in *A. africanus*, shearing of the anterior rostrum is reduced through the presence of bony struts that are loaded axially in compression. Columns function very efficiently in this regard, so much so that even the hollow strut represented by the anterior pillar substantially reduces strain magnitudes along the nasal margin. In contrast, during molar biting, compressive strains are oriented obliquely across the pillar. This is not a configuration that is structurally optimal, especially in comparison to strain orientations observed during premolar biting. These data do not obviously support (although they also do not definitively falsify) the hypothesis that the pillar evolved as a response to molar loading (Grine et al., 2010). Rather, the strain orientation data seem most compatible with the hypothesis that the pillar evolved to resist loads associated with premolar loading, and that this morphology has an ancillary effect of strengthening the face during all loading regimes. As several studies have shown that cortical bone is best modeled as orthotropic, meaning that mechanical properties vary in three mutually perpendicular planes defined by three principal axes (e.g., Ashman et al., 1984; Schwartz-Dabney and Dechow, 2002), further studies that incorporate the effects of this anisotropy may shed additional light on the deformation of the pillar under various loading regimes.

CONCLUSIONS

We find support for the hypothesis that both a straight/steep (expanded) zygomatic root and the presence of "anterior pillars" strengthen the face against feeding loads. However, we show that a reinforced face is not necessarily a strong face, with anterior positioning of the zygomatic root (and thus superficial masseter attachment) increasing strain magnitudes even in the presence of bony facial reinforcement features. The results suggest that an anteriorly placed zygomatic root complex evolved to enhance the efficiency of bite force production while other facial strengthening features, such as the anterior pillar and the straight/steep ZAC may have been selected for in part to compensate for the weakening effect of this facial configuration. However, the feeding mechanics of *Paranthropus boisei* (Smith et al., 2015a) demonstrates that australopiths may have been adapted to mechanically challenging diets along different evolutionary trajectories, perhaps because of the pre-existing constraints unique to each species. Future analyses of additional australopith species, as well as variation within australopith species, will continue to inform our understanding of early hominin biomechanical diversity.

ACKNOWLEDGEMENTS

The authors thank the Academic Editor and anonymous reviewers who provided helpful comments and critique on an earlier draft of this article.

LITERATURE CITED

Ashman RB, Cowin SC, Van Buskirk WC, Rice JC. 1984. A continuous wave technique for the measurement of the elastic properties of cortical bone. J Biomech 17:349–361.

Benazzi S, Nguyen HN, Kullmer O, Hublin J-J. 2013. Unravelling the functional biomechanics of dental features and tooth wear. PLoS One 8:e69990.

Benazzi S, Nguyen HN, Kullmer O, Hublin J-J. 2015. Exploring the biomechanics of taurodontism. J Anat 226:180–188.

Berger LR, de Ruiter DJ, Churchill SE, Schmid P, Carlson KJ, Dirks PHGM, Kibii JM. 2010. *Australopithecus sediba*: a new species of *Homo*-like australopith from South Africa. Science 328: 195–204.

Bookstein FL. 1991. Morphometric tools for landmark data: geometry and biology. Cambridge: Cambridge University Press.

Cerling TE, Mbua E, Kirera FM, Manthi FK, Grine FE, Leakey MG, Sponheimer M, Uno KT. 2011. Diet of *Paranthropus boisei* in the early Pleistocene of East Africa. Proc Natl Acad Sci USA 108: 9337–9341.

Daegling DJ, Judex S, Ozivici E, Ravosa MJ, Taylor AB, Grine FE, Teaford MF, Ungar PS. 2013. Feeding mechanics, diet, and dietary adaptations in early hominins. Am J Phys Anthropol 151: 356–371.

Davis JL, Dumont ER, DS, Strait DS, Grosse IR. 2011. An efficient method of modeling material properties using a thermal diffusion analogy: an example based on craniofacial bone. PLoS One 6: e17004.

Demes B, Creel N. 1988. Bite force, diet, and cranial morphology of fossil hominids. J Hum Evol 17:657–670.

Dumont ER, Grosse IR, Slater GJ. 2009. Requirements for comparing the performance of finite element models of biological structures. J Theor Biol 256:96–103.

Dumont ER, Samadevam K, Grosse IR, Warsi OM, Baird B, Dávalos LM. 2014. Selection for mechanical advantage underlies multiple cranial optima in new world leaf-nosed bats. Evolution 68:1436–1449.

Ellis EIII, El-Attar A, Moos KF. 1985. An analysis of 2,067 cases of zygomatico-orbital fracture. J Oral Maxillofac Surg 43:417–428.

Greaves WS. 1978. The jaw lever system in ungulates: a new model. J Zool 184:271–285.

Grine FE, Judex S, Daegling DJ, Ozcivici E, Ungar PS, Teaford M, Sponheimer M, Scott J, Scott RS, Walker A. 2010. Craniofacial biomechanics and functional and dietary inferences in hominin paleontology. J Hum Evol 58:293–308.

Grosse IR, Dumont ER, Coletta C, Tolleson A. 2007. Techniques for modeling muscle induced forces in finite element models of skeletal structures. Anat Rec 290A:1069–1088.

Gunz P. 2005. Statistical and geometric reconstruction of hominid crania: reconstructing australopithecine ontogeny. Ph.D. Dissertation, University of Vienna.

Hylander WL. 1977. The adaptive significance of Eskimo craniofacial morphology. In: Dahlberg AA, Graber TM, editors. Orofacial growth and development. Chicago, IL: Aldine Publishing Company. p 129–169.

Kimbel WH, Rak Y, Johanson DC. 2004. The skull of *Australopithecus afarensis*. Oxford University Press, Oxford.

Ledogar JA, Smith AL, Benazzi S, Weber GW, Spencer MA, Carlson KB, McNulty KP, Dechow PC, Grosse IR, Ross CF, et al. 2016a. Mechanical evidence that *Australopithecus sediba* was limited in its ability to eat hard foods. Nat Commun 7:10596.

Ledogar JA, Dechow PC, Wang Q, Gharpure PH, Gordon AD, Baab KL, Smith AL, Weber GW, Grosse IR, Ross CF, et al. 2016b. Human feeding biomechanics: performance, variation, and functional constraints. Peer J 4:e2242.

Lockwood CA. 1999. Sexual dimorphism in the face of *Australopithecus africanus*. Am J Phys Anthropol 108:97–127.

Lucas PW, Turner IM, Dominy NJ, Yamashita N. 2000. Mechanical defences to herbivory. Ann Bot 86:913–920.

McKee JK. 1989. Australopithecine anterior pillars: reassessment of the functional morphology and its phylogenetic relevance. Am J Phys Anthropol 80:1–9.

Panagiotopoulou O, Kupczik K, Cobb SN. 2011. The mechanical function of the periodontal ligament in the macaque mandible: a validation and sensitivity study using finite element analysis. J Anat 218:75–86.

Peters CR. 1987. Nut-like oil seeds: food for monkeys, chimpanzees, humans, and probably ape-men. Am J Phys Anthropol 73:333–363.

Prado FB, Freire AR, Rossi AC, Ledogar JA, Smith AL, Dechow PC, Strait DS, Voigt T, Ross CF. 2017. Review of in vivo bone strain studies and finite element models of the zygomatic complex in humans and non-human primates: implications for clinical research and practice. Anat Rec 299:1753–1778.

Rak Y. 1983. The australopithecine face. New York: Academic Press.

Rak Y. 1985a. Sexual dimorphism, ontogeny, and the beginning of differentiation of the robust australopithecine clade. In: Tobias PV, editor. Hominid evolution: past, present, and future. New York: Alan R. Liss, Inc. p 233–235.

Rak Y. 1985b. Australopithecine taxonomy and phylogeny in light of facial morphology. Am J Phys Anthropol 66:281–287.

Rak Y. 1985c. Systematic and functional implications of the facial morphology of *Australopithecus* and early *Homo*. In: Delson E, editor. Ancestors: the hard evidence. New York: Alan R. Liss, Inc. p 168–170.

Ross CF, Berthaume MA, Dechow PC, Iriate-Diaz J, Porro LB, Richmond BG, Spencer M, Strait DS. 2011. *In vivo* bone strain and finite-element modeling of the craniofacial haft in catarrhine primates. J Anat 218:112–141.

Ross CF, Iriarte-Diaz J. 2014. What does feeding system morphology tell us about feeding? Evol Anthropol 23:105–120.

Schwartz-Dabney CL, Dechow PC. 2002. Accuracy of elastic property measurement in mandibular cortical bone is improved by using cylindrical specimens. J Biomech Eng 124:714–723.

Scott RS, Teaford MF, Ungar PS. 2012. Dental microwear texture and anthropoid diets. Am J Phys Anthropol 147:551–579.

Smith AL, Benazzi S, Ledogar JA, Tamvada K, Pryor Smith LC, Weber GW, Spencer MA, Lucas PW, Michael S, Shekeban A, et al. 2015a. The feeding biomechanics and dietary ecology of *Paranthropus boisei*. Anat Rec 298:145–167.

Smith AL, Benazzi S, Ledogar JA, Tamvada K, Pryor Smith LC, Weber GW, Spencer MA, Dechow PC, Grosse IR, Ross CF, et al. 2015b. Biomechanical implications of intraspecific shape variation in chimpanzee crania: moving towards an integration of geometric morphometrics and finite element analysis. Anat Rec 298:122–144.

Spencer MA. 1999. Constraints on masticatory system evolution in anthropoid primates. Am J Phys Anthropol 108:483–506.

Stayton CT. 2009. Application of thin-plate spline transformations to finite element models, or, how to turn a bog turtle into a spotted turtle to analyze both. Evolution 63:1348–1355.

Strait DS, Constantino P, Lucas PW, Richmond BG, Spencer MA, Dechow PC, Ross CF, Grosse IR, Wright BW, Wood BA, et al. 2013. Diet and dietary adaptations in early hominins: the hard food perspective. Am J Phys Anthropol 151:339–355.

Strait DS, Richmond BG, Spencer MA, Ross CF, Dechow PC, Wood BW. 2007. Masticatory biomechanics and its relevance to early hominid phylogeny: an examination of palatal thickness using finite-element analysis. J Hum Evol 52:585–599.

Strait DS, Weber GW, Constantino P, Lucas PW, Richmond BG, Spencer MA, Dechow PC, Ross CF, Grosse IR, Wright BW, et al. 2012. Microwear, mechanics and the feeding adaptations of *Australopithecus africanus*. J Hum Evol 62:165–168.

Strait DS, Weber GW, Neubauer S, Chalk J, Richmond BG, Lucas PW, Spencer MA, Schrein C, Dechow PC, Ross CF, et al. 2009. The feeding biomechanics and dietary ecology of *Australopithecus africanus*. Proc Natl Acad Sci USA 106:2124–2129.

Teaford MF, Ungar PS. 2000. Diet and evolution of the earliest human ancestors. Proc Natl Acad Sci USA 97:13506–13511.

Ungar PS, Scott RS, Grine FE, Teaford MF. 2010. Molar microwear textures and the diets of *Australopithecus anamensis* and *Australopithecus afarensis*. Phil Trans R Soc B 365:3345–3354.

Villmoare BA, Kimbel WH. 2011. CT-based study of internal structure of the anterior pillar in extinct hominins and its implications for the phylogeny of robust *Australopithecus*. Proc Natl Acad Sci USA 108:16200–16205.

Weber GW, Krenn V. 2017. Zygomatic root position in recent and fossil hominids. Anat Rec 300:160–170.

Wright BW. 2005. Craniodental biomechanics and dietary toughness in the genus *Cebus*. J Hum Evol 48:473–492.